To the Graduate Council:

I am submitting herewith a thesis written by James Jack DiCillo entitled " Optical Limiters For Eye And Sensor Protection From Lasers." I have examined the final copy of this thesis for form and content and recommend that it be accepted in partial fulfillment of the requirement for the degree of Master of Science, with a major in physics.

Alvin J. Sanders, Major Professor

We have read this thesis and recommend its acceptance:

Marianne Breinig

Robert DeSerio

Alvin J. Sanders

Accepted for the Council:

Associate Vice Chancellor
and Dean of The Graduate School

OPTICAL LIMITERS

FOR EYE AND SENSOR PROTECTION FROM LASERS

A Thesis

Presented for the

Master of Science

Degree

The University of Tennessee, Knoxville

James Jack DiCillo

August, 1992

DEDICATION PAGE

This thesis is dedicated to my wife Denise for her loving support and patience, and to my parents, James and Celestina, for their encouragement and support.

ACKNOWLEDGEMENTS

I would like to thank my major professor, Dr. Alvin Sanders, for his valuable advice. I would also like to thank the other committee members, Dr. Mariane Breinig and Dr. Robert DeSerio, for their help and suggestions. I would like to express my gratitude to Dr. William Garrett, Dr. Marvin Payne, Ron Phillips, Steve Allman, Bill Brandon, and Brian Hasson for their generous assistance and constructive discussions. Finally, I would like to express my deepest appreciation to Dr. C.H. "Winston" Chen, for his advice, patience, assistance, and friendship.

ABSTRACT

This research investigated the feasibility of using thin film aluminum mirrors or phthalocyanine dyes to develop an optical limiting system to protect eyes and sensors from laser light. The mirrors are tested with laser light of 532 nanometers, in the middle of the visible spectrum. The dyes are tested with a dye laser to examine their effectiveness throughout the visible spectrum. Data are collected electronically and analyzed with a personal computer. Results indicate that separately, neither the mirrors nor the dyes attain the desired criteria. When combined in one optical system, results indicate that the desired level of protection is attainable. It is therefore possible to design an apparatus which will make use of these results to achieve the desired protection.

TABLE OF CONTENTS

LIST OF FIGURES

CHAPTER 1

INTRODUCTION

Background

Eye protection from bright flashes of light has been the subject of considerable research since the above ground nuclear tests of the 1950's. The development of the laser in 1960 produced a new threat to human eyes and optical sensors. By the early 1970's, the US military determined that eye protection from lasers was an important research goal. Presently, lasers on the battlefield fulfill such purposes as target designation, range finding, laser radar (LIDAR), and remote sensing. Eye protection for soldiers from these lasers becomes critical. In the near future, within five to ten years, it is expected that tunable lasers will also be used on the battlefield.

Eye protection from tunable lasers is difficult to achieve, since tunable lasers can emit light over a broad range of frequencies, albeit only one at a time. Protection must be developed to prevent damage to eyes and sensitive optical equipment. Specific applications for an eye protection device include tank windows and targeting telescopes.[1] It is a challenging task to provide protection from wavelength tunable lasers without the sacrifice of vision capability. Because the high intensity laser light must be eliminated without hindering normal viewing, an approach that is based on protection against individual wavelengths will not be very effective. Therefore, the approach presented in this thesis is to develop protection based solely on the intensity of light.

Since individual laser characteristics cannot be anticipated on the battlefield, it would be inappropriate to devise a defense which is tailored for one or even several lasers. The optimal solution is to determine the characteristics of those lasers that are most likely to be used on the battlefield and then adapt defensive measures for them. It is probable that these visible lasers will be pulsed with pulse lengths in the picosecond to microsecond range and that the energy incident on the target will be on the order of 10 to 1000 mJ. In general, attenuation of the laser pulse to allow a maximum incident energy of 10 μJ on the eye or sensor will provide sufficient protection. To accomplish this, an optical limiter must be used. The behavior of an optical limiter is shown in figure 1.1. A limiter allows transmission of light until an intensity threshold has been reached. Beyond that threshold, the transmitted intensity or energy remains constant.

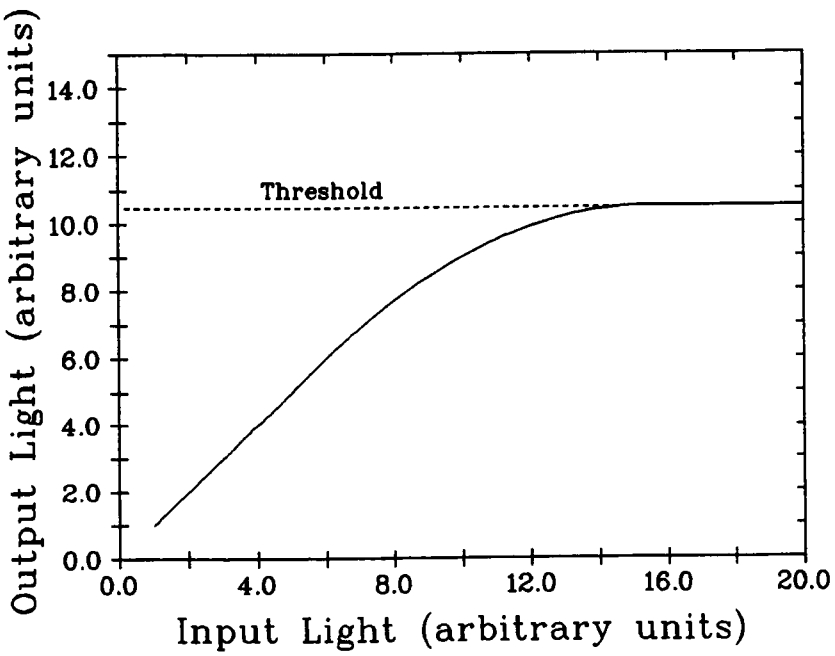

Figure 1.1. Behavior of an optical limiter.

Optical Requirements

The goal of these experiments is to find an optical limiter that attenuates light to an extent that there is minimal or no damage to the eye or optical system . The primary concern is protection from ultrashort (picosecond and nanosecond) laser pulses. Several studies in the past have determined that the damage done to the retina from an ultrashort pulse ($<$ 1 nanosecond) are not thermal in nature, but are caused by nonlinear effects, such as acoustic wave generation or multiphoton absorption[2-6]. Previous studies of eye damage from lasers have differed in the determination of the threshold retina damage level[2-14]. These differences are due to several factors, including different laser wavelengths and pulse durations, the determination of the focal spot size on the retina, and the definition of threshold retinal damage.

There are two ways that laser light can be incident on a target. Interbeam viewing is means that the entire beam is incident on the eye or optical device. Extended source viewing happens when a laser beam has diverged to a great extent or has scattered before being incident on the target. The image size on the retina to be expected is that of an extended source, as the possibility of this type of viewing is more likely on the battlefield than interbeam viewing. The ANSI standards[15] state that for visible wavelengths and nanosecond pulse durations, the maximum permissable exposure on the surface of the cornea is $\approx$ 0.5 μJ. Damage begins to occur at ten times that level, or at an irradiance of 5 μJ. In fact, the damage threshold caused by nanosecond pulse lasers on rhesus monkey retinas has been determined to be on the order of 2 to 9 μJ[5]. A sample of the research concerning eye damage is presented in table 1.

Table 1. Summary of Damage Thresholds from Q-switched lasers operating with nanosecond pulse lengths.

YEAR	RESEARCHER	DAMAGE THRESHOLD (μJ)
1972	Ham[4]	65
1973	Goldman[4]	18.2
1973	Gibbons[7]	3.0
1974	Ham[4]	8.7
1975	Taboada[2]	2.2
1978	Taboada[3]	3.5
1980	Bruckner[5]	2.1
1984	Welch[13]	12.7
1985	Allen[14]	2.0

Previous Work

Eye and sensor protection devices can be divided into two categories. These are indirect or direct viewing systems. Indirect viewing systems are those that monitor incident light with a remote system; a camera and television monitor. Indirect viewing systems include liquid crystal light valves[16], saturable amplifier power limiters, and saturable fluorescence power limiters[17]. Liquid crystal light valves make use of an

induced birefringence and are essentially optical-to-optical transducers. The image that is seen is isolated from the outside light and is produced by a separate light source. Saturable amplifier power limiters amplify all incoming signals to the same level. Then, the light is attenuated to a safe level. All light in the presence of a laser pulse will be at the same intensity, and then will pass through a neutral density filter. Saturable fluorescence power limiters have intensity-dependent absorption coefficients when a certain threshold is reached in the presence of high-intensity light. The drawback to these and other indirect viewing devices is that they are large and bulky. Incorporation into a compact model which does not interfere with battlefield maneuverability is difficult. They also require external power sources which make their application in battlefield vehicles somewhat limited.

Direct viewing systems are those that allow the incident light to strike the eye or sensor. Direct systems include both active and passive devices. Active devices require a trigger to activate them, while passive devices attenuate light by nature of their inherent material characteristics. Direct active devices include electrochromic optical switches, liquid crystal switches, and photochromic optical switches[17]. Electrochromic optical switches use transition metal oxides, such as WO_3 and V_2O_5. The optical density of these materials will change when subjected to an electric field. Liquid crystal switches have a liquid crystal sandwiched between two crossed polarizers. When light of normal intensity is incident, the crystals are oriented to allow light to pass through the system. When the light becomes intense, the crystals align themselves so no light passes through. The disadvantage with these devices is their slow response times, on the order of 100 to

1000 microseconds.

Direct passive devices which seem to have the greatest promise are nonlinear waveguides[18], nonlinear absorbing polymers[19], dynamic absorbing filters[17], and monolithic semiconductors[20]. Nonlinear waveguides pass light through the system until a threshold intensity has been reached. Above that threshold, light begins to tunnel into a nonlinear polymer which surrounds the transparent material. Doped nonlinear absorbing polymer films such as polycarbazole use the delocalization of charges in excited states to stimulate broadband absorption in the visible spectrum. Dynamic absorbing filters use organic dyes, such as those based on anthraquinone. These dyes exhibit intensity limiting behavior at certain intensity levels. Two drawbacks with these devices are the wavelength limited response and the intensity level response. Monolithic semiconductors make use of a tiny pinhole through which light is focussed. When intense light is focussed at the pinhole, a certain amount of defocussing occurs and damage results in the surrounding material. The disadvantages with this device are the high power density required to achieve defocussing and the destruction of the material[20].

Present Work

A direct passive device using a combination of damageable components and nonlinear absorption has been designed, tested, and has shown to have promising results. The damage components consist of thin-film mirrors arranged in a novel optical design. The nonlinear absorption has been achieved by using organo-metallic dyes. Chapters 2 and 3 will discuss the sacrificial mirror method. Chapters 4 and 5 will elucidate the

nonlinear absorbing dye solution.

CHAPTER 2

SINGLE-PASS REFLECTION EXPERIMENTS

Background

The use of thin film aluminum mirrors for laser eye protection has been studied previosly[17,21,22]. The interaction of these mirrors with lasers has also been studied in the field of laser fusion[23-25]. When a laser pulse is focussed on the surface of such a mirror, the metal surface of the mirror is vaporized by part of the pulse, leaving a hole in the mirror. The rest of the laser pulse will then travel through the mirror rather than be reflected from it into the viewing system. If the damage to the mirror occurs swiftly enough, the attenuation of the laser pulse will be significant. However, none of the previous work has shown that a single sacrificial mirror can attenuate light below the eye damage threshold. The single-pass reflection experiments conducted in this study indicate that the use of a single sacrificial mirror is inadequate.

Various parameters that can affect attenuation such as laser power density, metal film thickness, laser wavelength, and mirror damage thresholds are also examined. A simple estimate of the attenuation to be expected can be calculated, assuming a square pulse shape with duration of 7 ns. The velocity of desorbed particles and plasma created by the ablation process has been measured by previous investigators at 10^7 cm/s in vacuum[23,24,26]. Since the present work was done in air, the average velocity of the desorbed materials is assumed to be on the order of 10^5 cm/s. Because the thickness of

the aluminum films is only 500 Å, a displacement of the surface by 100 nm can be assumed to reduce reflectivity to a minimal level. The time required to destroy the reflectivity of the surface of the mirror will then be on the order of 100 nm $\div$ 10^5 cm/s = 100 ps. Therefore, the attenuation of the pulse from a single reflection should be at a minimum, 7 ns $\div$ 100 ps, or $\approx$ 70.

Equipment

The laser used is a Quanta Ray DCR Nd:YAG multimode Q-switched pulsed laser with a beam divergence of 0.5 milliradians. The laser pulse length is 7 nanoseconds and the beam is frequency doubled to produce 532 nm light. The spatial beam quality is measured with a linear photodiode array and the data is stored and printed out with a DL 2140B digital oscilliscope. Figure 2.1 shows the spatial intensity of a cross section of the beam at various times after the laser is started. As can be seen in figure 2.1.c, after approximately one hour, the beam quality is quasi-guassian. The laser lamps operate at the optimal repitition rate of 10 Hz. The Q-switch is activated once every five seconds synchronously with the lamps using an external coincidence unit with a digital counter and delay. Incident laser power is measured with a Coherent 210 power meter. Reflected power from the aluminum mirrors is measured with both a Gentec ED-100A joulemeter connected to a Tektronix 2235 100 MHz oscilloscope and a photodiode connected to a signal sample and hold unit interfaced with a personal computer. Figures 2.2 and 2.3 show the calibration graphs for the photodiode and the Gentec energy meter.

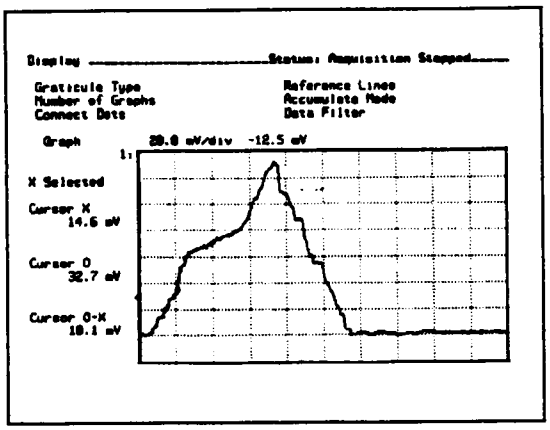

a)

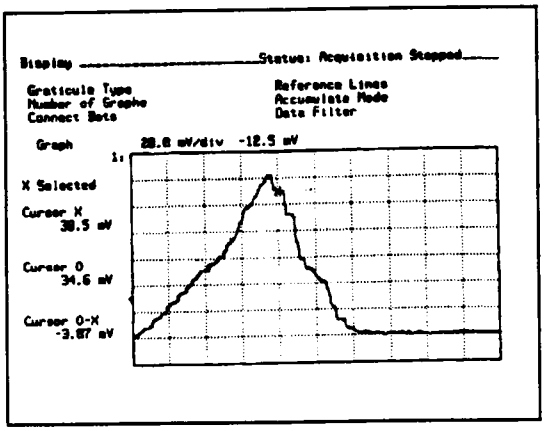

b)

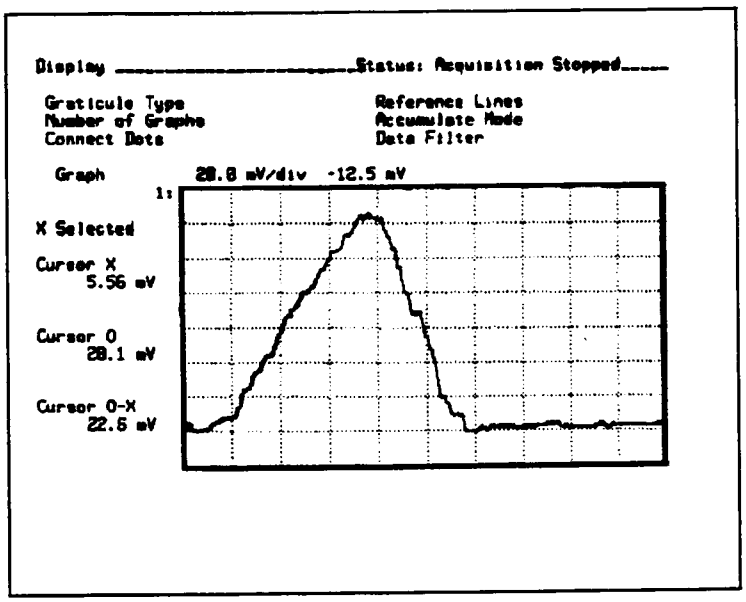

c)

Figure 2.1. Laser beam spatial profiles. a) Profile after laser was operating for 1 minute. b) Profile after 5 minutes. c) Profile after 1 hour. Horizontal axes are distances across the beam and the vertical axes are the beam intensities.

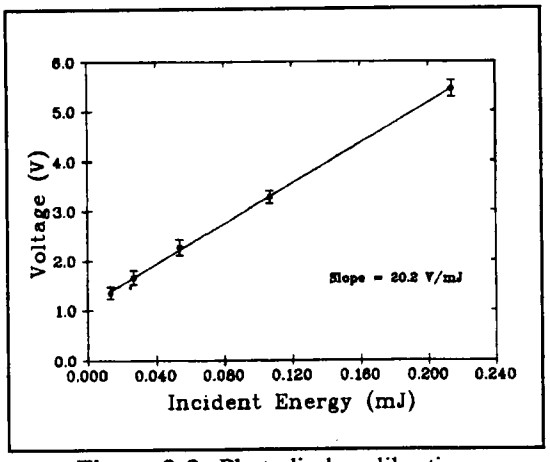

Figure 2.2. Photodiode calibration.

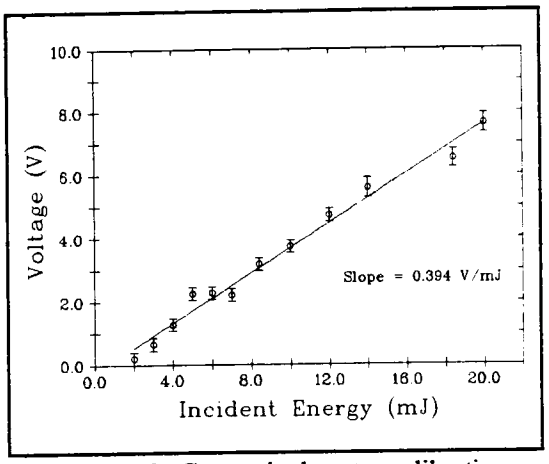

Figure 2.3. Gentec joulemeter calibration.

Several types of temporary mirrors were used. Fabricated mirrors are made from films consisting of 100 nm of aluminum coated on a clear mylar backing with a thickness of 2.5 microns. These films are mounted on copper rings and stretched to form mirrors. The reflectivity of these mirrors was measured to be 85% at 532 nm. Purchased mirrors were obtained from National Photocolor Corporation. These mirrors are made from black-dyed mylar with a thickness of 2.5 microns and 500 Å of aluminum coating. The reflectivity of purchased mirrors was measured to be 95% at 532 nm.

Experiment

The schematic of the single reflection experiment is shown in figure 2.4. The Al film mirror is mounted on an x-y-z translator. This allowed repositioning of the mirror after each laser shot. During translation, the laser pulse is focussed onto the surface of a the mirror while the laser is operating at 10 Hz without being Q-switched. This enabled minor position adjustments to be made without damaging the mirror. Then the

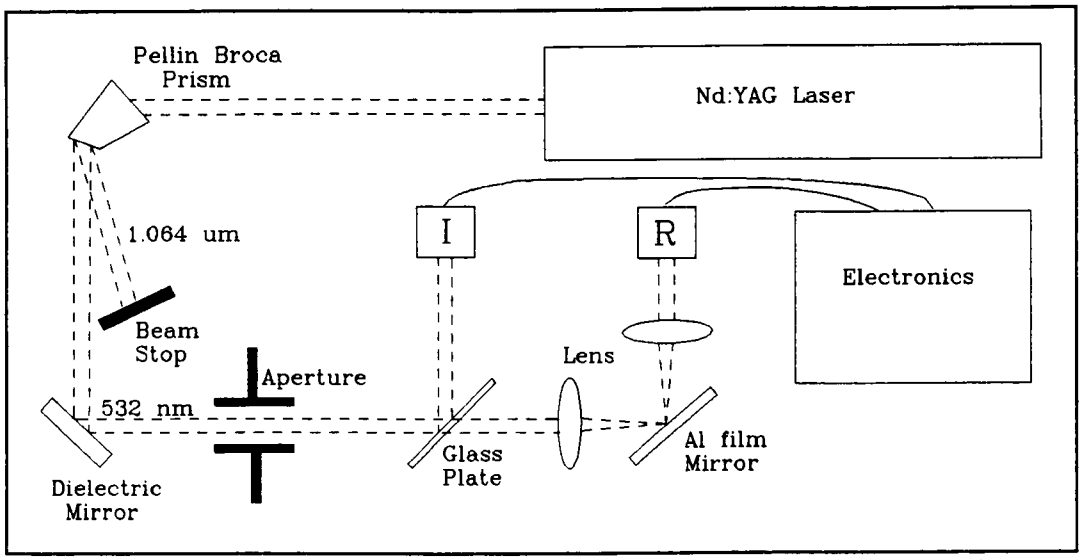

Figure 2.4. Single reflection experimental schematic. I is the incident laser energy. R is the reflected laser energy.

mirror is subjected to a single Q-switched pulse. The amount of light reflected from the mirror is recorded with incident energies ranging from 0.625 mJ to 100 mJ. Lenses of 5, 20, and 100 cm focal lengths are used. In figure 2.5, data from several different trials with different focal length lenses are plotted. The best-fitting straight lines are also plotted with the data. The results show that the light reflected from the mirror is significantly decreased when the focal length of the lens is reduced. The light reflected is considerably less with a 5 cm lens as compared with a 100 cm lens. The maximum attenuation of the incident laser pulse energy achieved ranged from 50 to 100 using a 5 cm lens. The results obtained are consistent with those from previous studies after experimental differences are accounted for[17,25,26]. Error bars are not included with the graphs because the purpose of these experiments is to determine the general response of the thin film mirrors to laser light, not to make an exact measurement of reflected light.

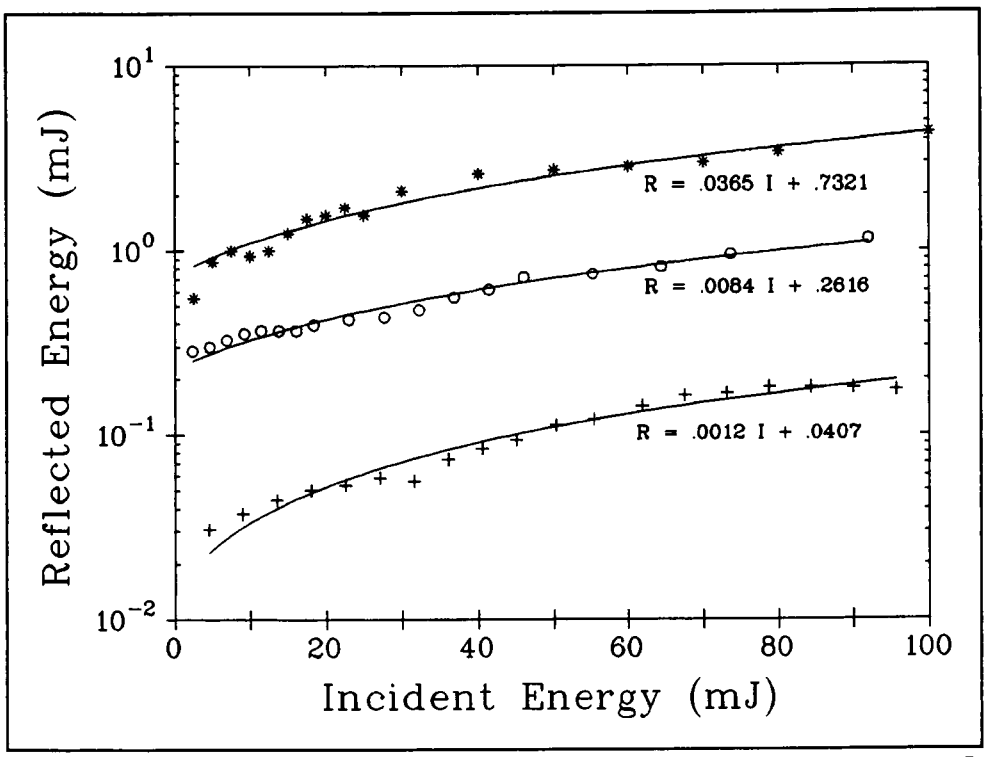

Figure 2.5. Single reflection results. (*) = 100 cm lens, (o) = 20 cm lens, (+) = 5 cm lens. Fitted lines which are linear least-squares fits of R vs I for I > 2.5 mJ are also displayed.

Modifications of Single-Pass System

To determine if the attenuation of light could be increased, a second Al mirror is placed between the first mirror and the detector (figure 2.6). After the light is reflected from the first mirror, it is focussed onto the surface of the second mirror with a 20 cm focal length lens and then focussed onto the detector with a 5 cm focal length lens (figure 2.6). The attenuation is increased by a factor of three. An examination of damage spots on the mirrors revealed that although the size of the damage spots on the first mirror increases with increasing laser power, the size of the damage spot on the second mirror remains constant. Therefore, only the first mirror substantially limits the output of the

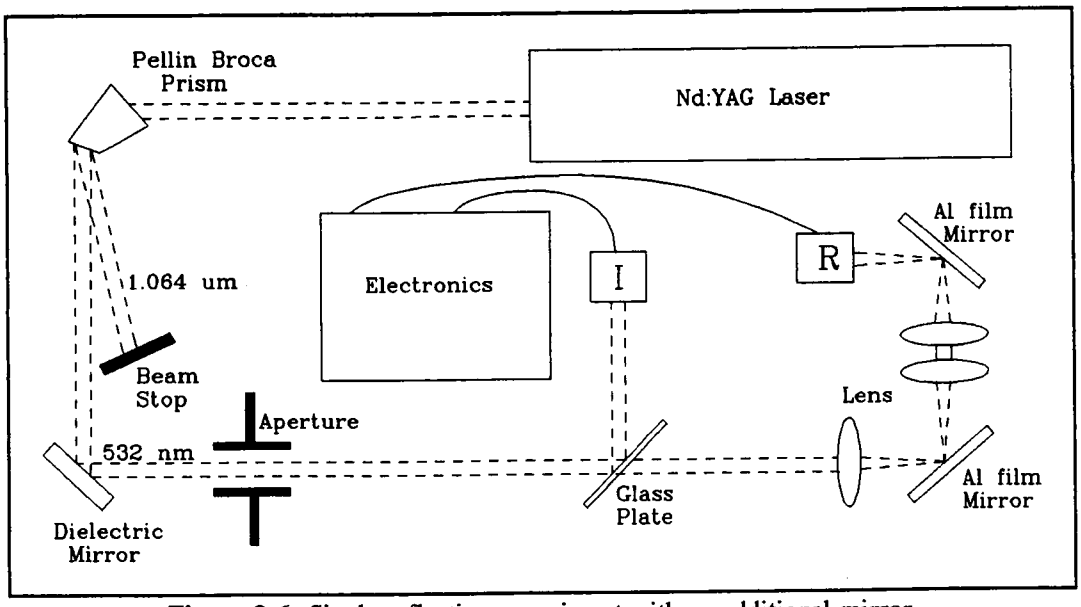

Figure 2.6. Single reflection experiment with an additional mirror.

reflected laser pulse. The second mirror is not visibly damaged when the focal length of the lens focussing light onto the first mirror is less than 10 cm. Apparently not enough light is reflected from the first to the second mirror to cause an onset of damage. The damaged area on the second mirror reaches a maximum size when the focal length of the first lens is 20 cm.

As a second modification, the single reflection experiment is performed in a vacuum chamber. The motivation was that the rate of thermal conduction along the surface of the film is higher in a vacuum. Increased heat dissipation from the focal spot on the mirror can cause the ablation process to occur more swiftly. The experiment is conducted both at room pressure and at 5.9 x 10^{-5} atmospheres. The amount of light reflected from the mirror at low pressure is greater than at ambient pressure (figure 2.7). The size of the damage spots on the mirror is consistently larger in vacuum than at atmospheric pressure (figure 2.8).

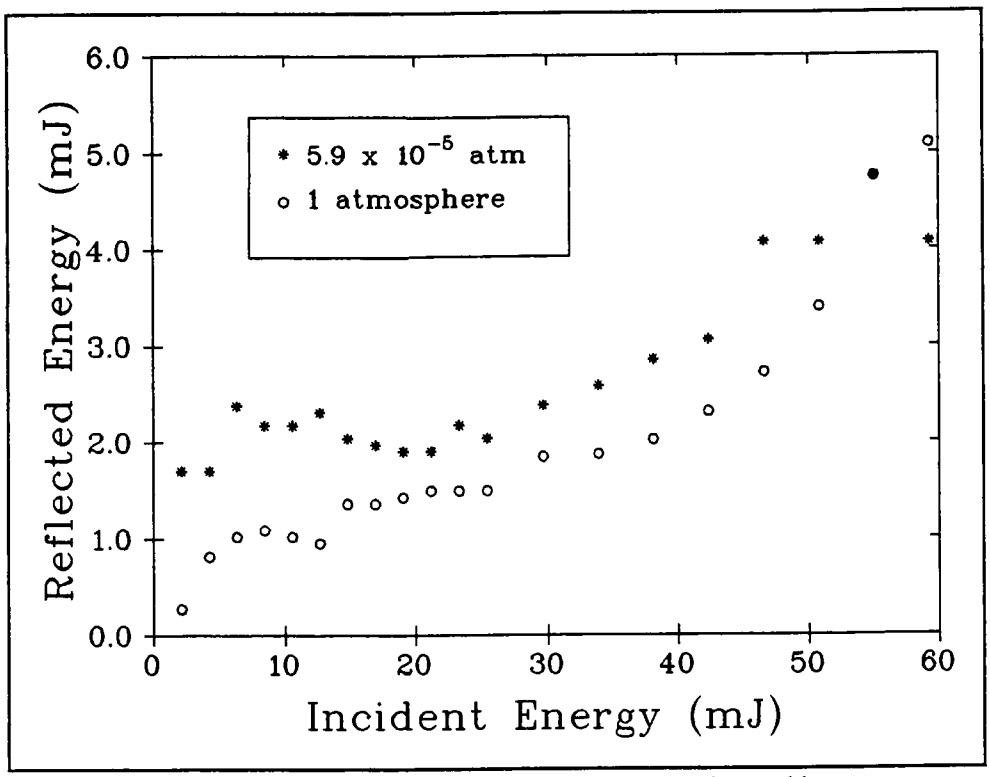

Figure 2.7. Comparison of reflected energy in vacuum and at ambient pressure.

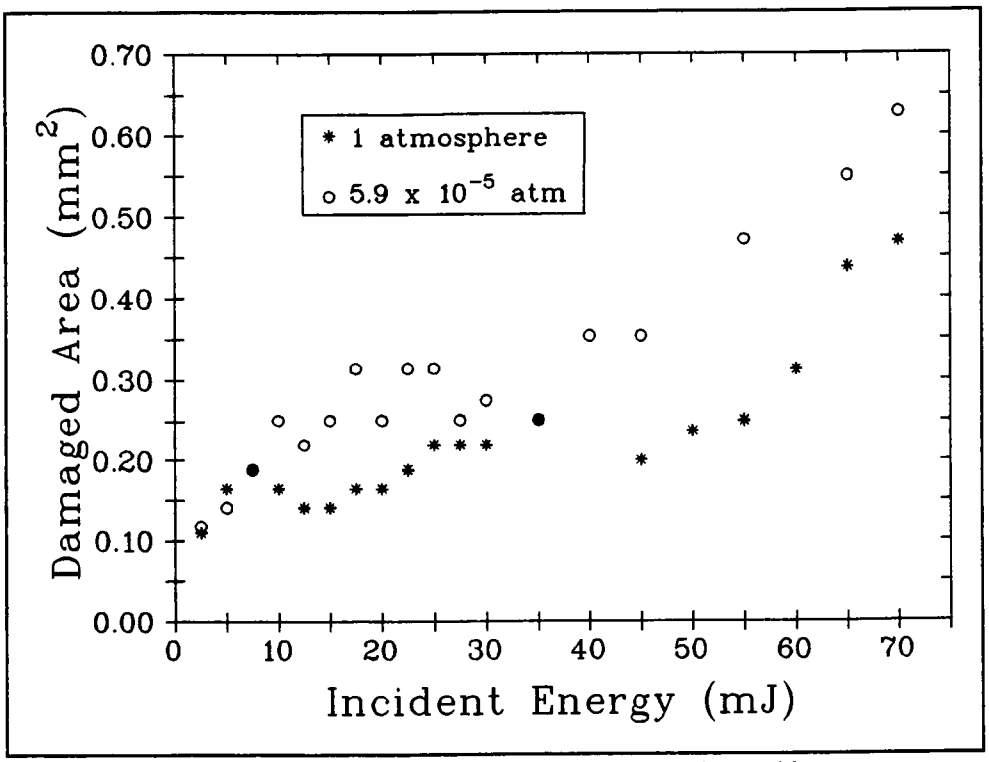

Figure 2.8. Comparison of damaged areas in vacuum and at ambient pressure.

At this stage, the burn-through threshold of the purchased aluminum mirrors is measured by attenuating the laser pulse until the smallest amount of visible damage is observed. This occured at an energy of 0.13 μJ. The theoretical value of this threshold energy is 0.299 μJ (Appendix A).

Results

The amount of light reflected from a single pass at a temporary mirror has been determined to be greater than allowed by the established criteria. This is shown in figure 2.5. The introduction of a second temporary mirror did not reduce the reflected light to an acceptable level. In vacuum, the reflected light is greater than at ambient pressure. Damage spot sizes are smaller in vacuum. This is due to the fast movement of ablated material away from the surface, which allows less heat conduction to aluminum around the focal spot. The single reflection approach is therefore not an acceptable attenuation mechanism. This conclusion is in agreement with previous studies[17,21,22]. Consequently, a double-pass optical sytem was tested, the results of which are explained in chapter 3.

CHAPTER 3

DOUBLE-PASS REFLECTION EXPERIMENTS

Background

The experiments described in chapter 2 showed that with a single-pass optical system, regardless of whether it employed a second mirror or not, the attenuation of laser light below the eye damage threshold can not be accomplished. Therefore, a double-pass system was designed in order to achieve a greater attenuation of the incident light. This optical system was designed as illustrated in figure 3.1. Part of the laser pulse is reflected from the surface of the first mirror before damage can occur. This configuration returns that light to that damaged spot. If the damage mechanisms occur swiftly enough, then the light will pass through the damaged area and not be reflected back to the detector or to the eye. The attenuation for a single reflection was estimated to be a factor of 70 (chapter 2). Therefore, the minimum attenuation expected from a return pass through the mirror can be expected to be at least 70^2, or approximately 5000.

The incident laser pulse travels through a beam splitter and then is focussed with a 5 cm lens onto the first mirror. The light reflected from the first mirror passes through another 5 cm lens and is perpendicularly incident on a normal front surface mirror. This mirror reflects the light back to refocus on the thin film mirror at the origional focal spot. The light then returns to the beam splitter and the detector. When the mirror becomes damaged by the laser pulse, light should not return to the detector.

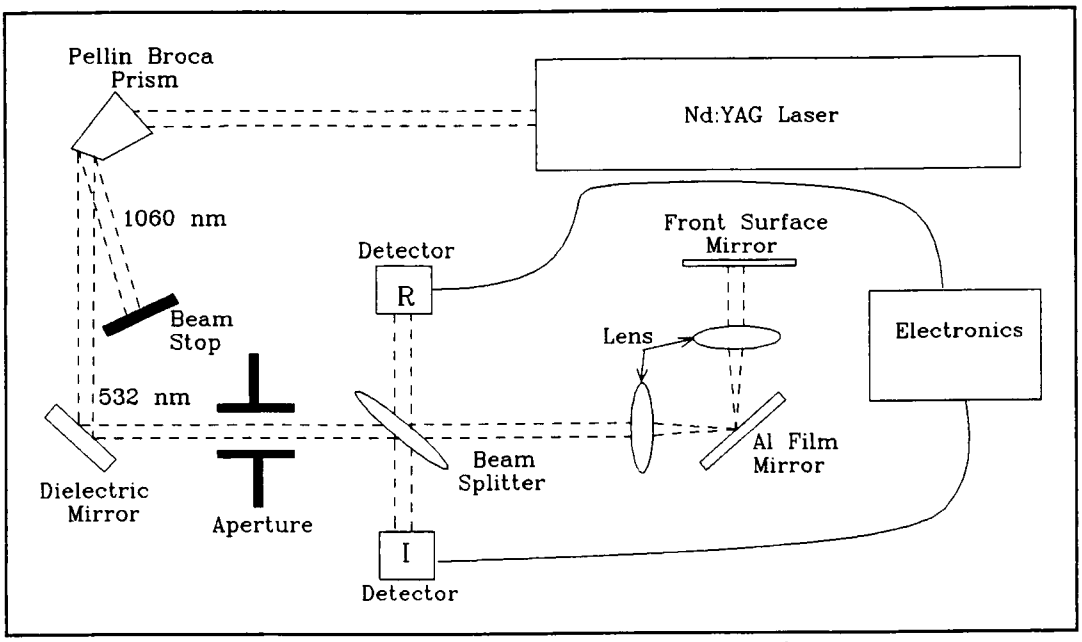

Figure 3.1. Schematic for double reflection experiments.

Experiment

The equipment used for the double reflection experiment was the same as for the single reflection experiment. The results depicted in figure 3.2 show a peak energy transmittance of 31 μJ for the purchased mirror (dyed backing). The results also indicate that a maximum amount of reflected laser light occurs between 20 and 30 millijoules of incident energy. For the purchased mirrors, the mirror is fractured with a single shot at energies higher than 35 mJ. At 40, 45, and 50 mJ, zero reflected laser energy was recorded. Data from lower incident energies is plotted in figure 3.3. The results from the fabricated mirrors are plotted in figure 3.4. With one trial, the back of a fabricated mirror was painted black, so that the substrate would absorb more of the laser pulse. The graph shows that the same trend of a peak in the region of 20 - 25 mJ occurs with fabricated mirrors. However, the purchased mirrors reflect much less light than the fabricated mirrors, as is shown in figure 3.5. Several factors are assumed to be

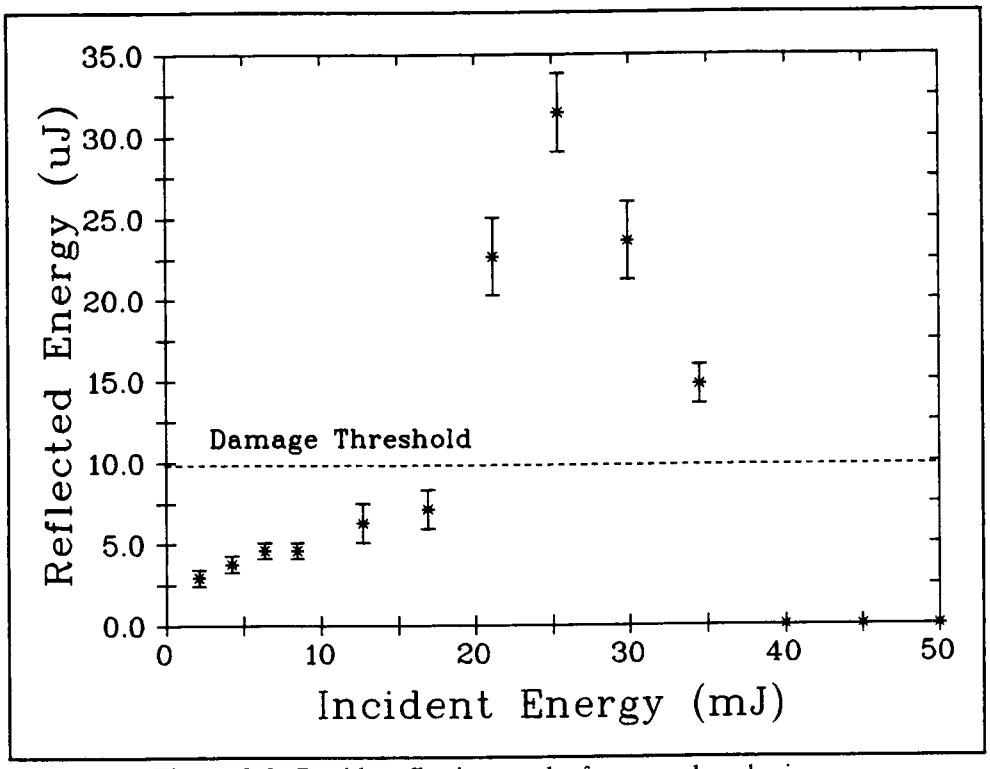

Figure 3.2. Double reflection results for a purchased mirror.

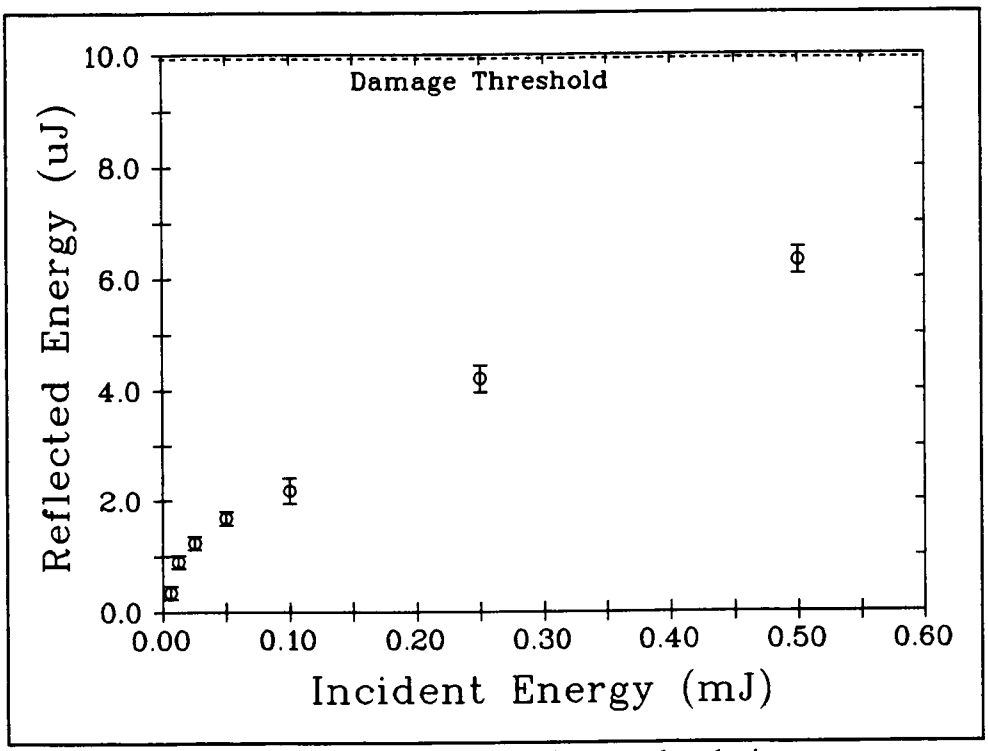

Figure 3.3. Low energy results for a purchased mirror.

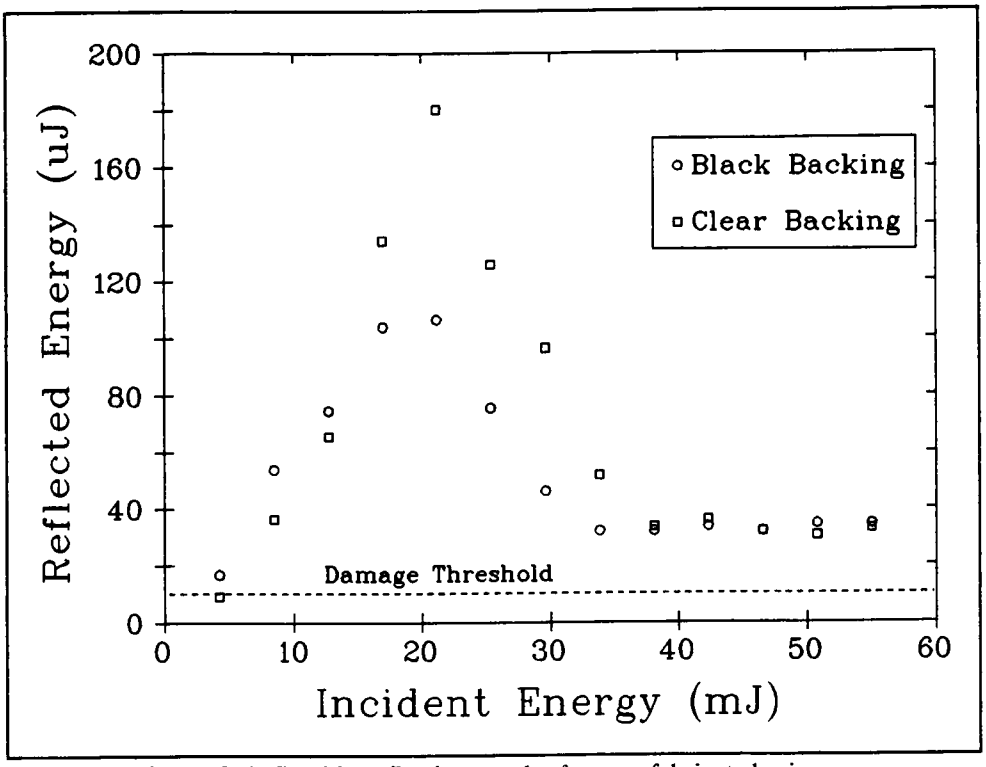

Figure 3.4. Double reflection results for two fabricated mirrors.

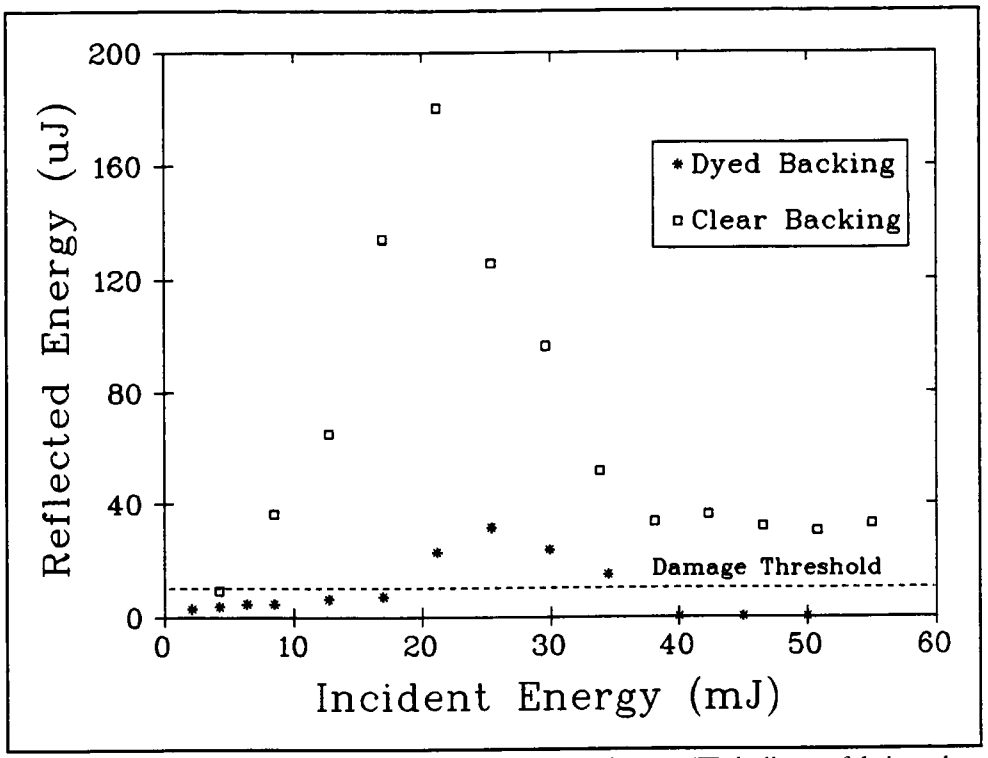

Figure 3.5. Double reflection results for both type mirrors. (□) indicates fabricated mirror and (*) indicates purchased mirror.

responsible for the low attenuation (figure 3.6), including the reflectivity of the plasma produced and the possibility that surface damage is not occurring quickly enough to attenuate the pulse. As with the single reflection data, error bars were not included with the fabricated mirror results.

The time that the damage process takes to occur is critical for the success of this double-pass reflection configuration. If, by the time the initial part of the laser pulse returns to the first mirror, the damage has not yet rendered the mirror into a poor reflector, then there will be a large amount of light reflected back to the detector. This was tested by adjusting the time interval between the front part of the laser pulse leaving and returning to the first mirror. The time interval was changed by varying the distance

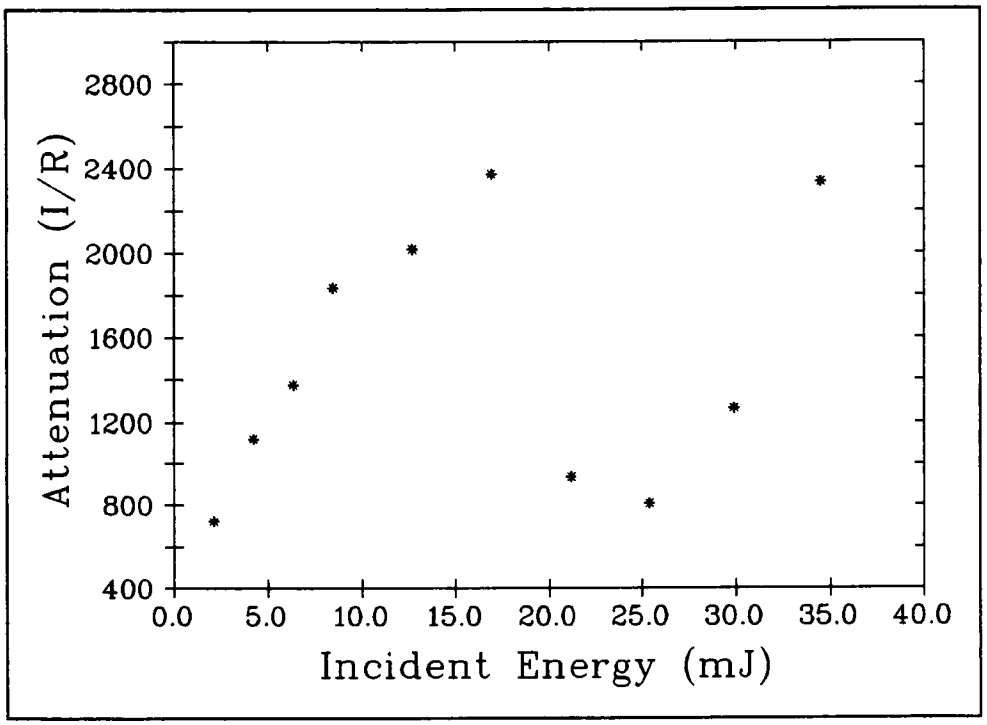

Figure 3.6. Attenuation of a purchased mirror. I is the incident energy and R is the reflected energy.

between the two mirrors. The experiment was conducted with distances of 40 cm and 240 cm between the two mirrors. These corresponded to 1.3 ns and 8 ns respectively. The results indicate that less light is reflected through the system with the longer distance (Fig. 3.7).

Measurement of Damaged Area

The damage areas were measured by two methods. The first was to examine the mirror under a microscope and measure the diameter of the holes with a reticle. An examination of the damage spots revealed that for fabricated mirrors, the mylar substrate was only burned through at the focal spot, although the area from which aluminum was

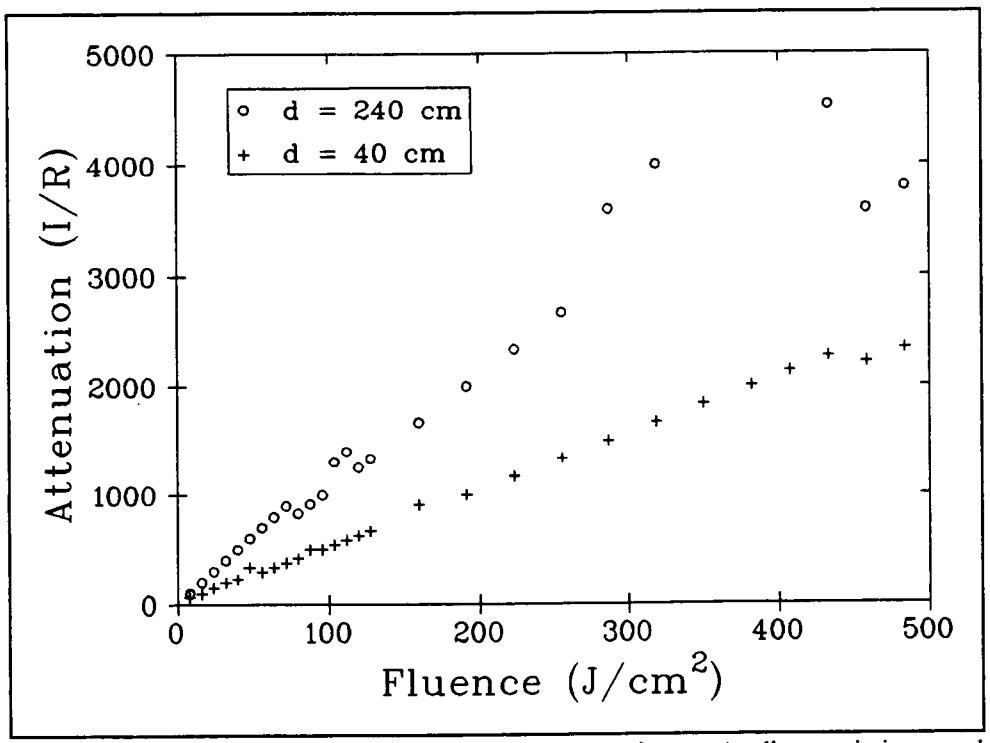

Figure 3.7. Distance variation for single reflection experiment. As distance is increased, attenuation is increased and reflected energy is decreased.

ablated was much greater. For the purchased mirrors, both the dyed substrate and aluminum film were completely gone. Since the black-dyed mylar must then absorb much more light than the clear mylar, the contribution of reflected light by the substrate is substantially reduced with the purchased mirrors.

Secondly, the hole diameter was estimated by measuring its diffraction pattern. A Helium Neon laser was passed through the damage spot, and the diffraction pattern created by the hole was projected onto a screen some distance away. This diffraction pattern is similar to an Airy disk[27]. The damaged areas were circular, but the edges of the circle were not uniform. This accounted for a variance in the measurement of the hole diameter by as much as 5%. The size of the Airy disk which would be produced by a perfectly circular hole is related to the hole size by the equation:

$$\sin(\theta) = \frac{1.22\,\lambda}{d}. \qquad (3-1)$$

λ is the laser wavelength, 633 nm. d is the hole diameter. θ is the inverse tangent of (r/x), where r is diameter of the first minimum and x is the distance between the mirror and the screen. The schematic for this procedure is illustrated in figure 3.8. The difference between the two types of measurement was minimal. The relationship of

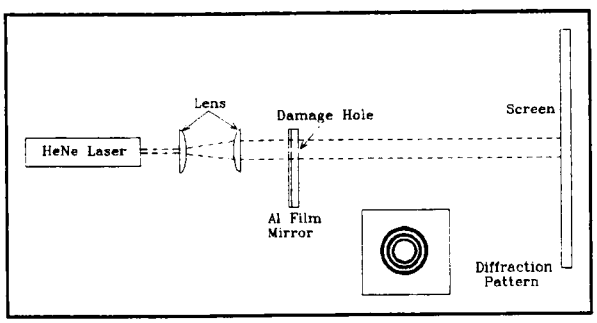

Figure 3.8. Schematic of method to measure damaged areas.

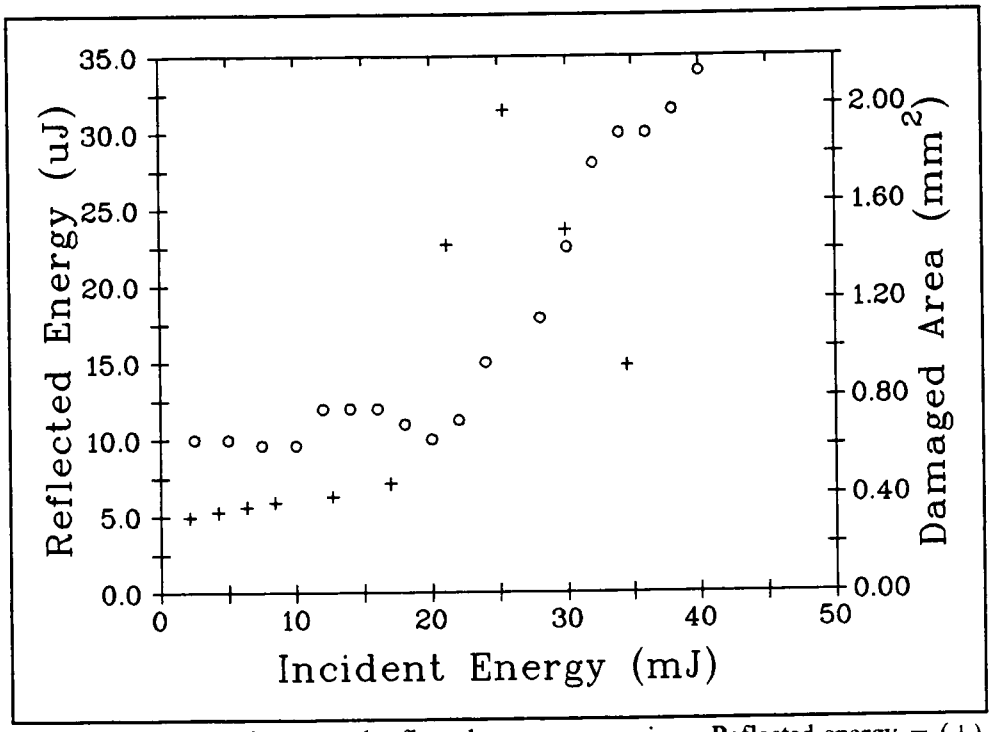

Figure 3.9. Damaged areas and reflected energy comparison. Reflected energy = (+) and damage areas = (o) for purchased mirror.

the damaged area to the reflected light is shown in figure 3.9. The onset of explosive damage, indicated by the sharp increase in damaged area at an incident energy of 20 mJ, approximately coincides with the decrease in reflected light at 25 mJ.

Measurement of Burn-through Times

In order to determine whether the simple estimate for the expected attenuation done at the beginning of chapter 2 is correct, another experiment was performed to determine the burn-through times of the films at various energies. The schematic for this experiment is shown in figure 3.10. Similar measurements have been made in the past using both double torsion pendulums[25,28] and ballistic pendulums[29]. A single torsion pendulum is constructed using 6 mil tungsten wire as the support for the mirror. A Helium Neon laser beam is aimed at a small mirror that is attached to the ring mount of

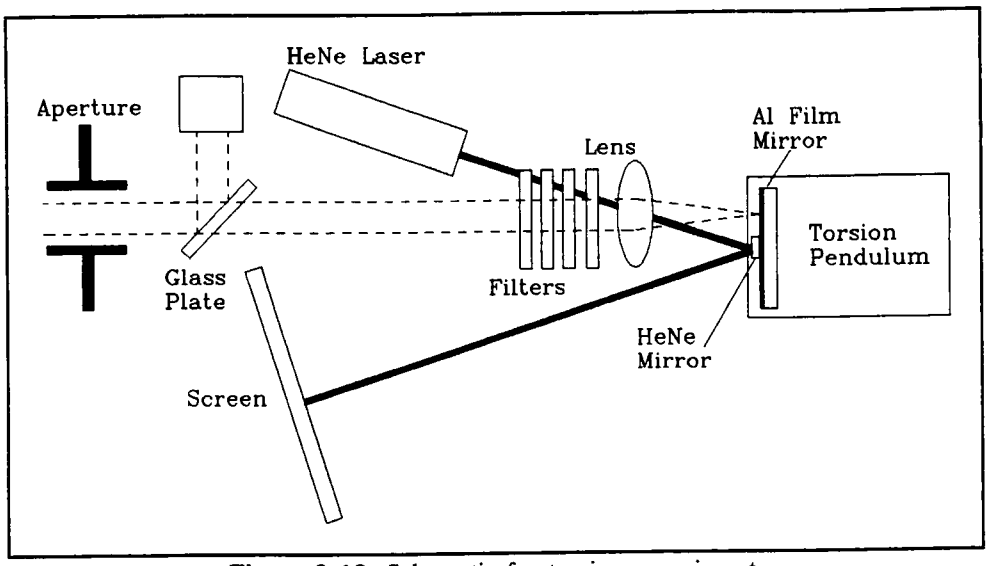

Figure 3.10. Schematic for torsion experiment.

the aluminum mirror. The Nd:YAG laser is operated in a single shot mode and the pulse is focussed at the surface of the aluminum mirror. The reflected beam is then projected onto a screen several meters distant. When the YAG laser is fired, the mirror rotates a small angle, θ. This causes an image of the HeNe laser on the screen to move a distance, l. The angle θ is calculated by:

$$\theta = 2 \tan^{-1} (l/x),$$

where x is the distance between the screen and the mirror. The distance between the hole in the mirror and the axis of rotation of the mirror is also measured.

The burn-through time is related to the angle of rotation of the mirror, the distance between the focal spot and the center of the mirror, and the incident energy on the mirror. The derivation of the relationship to calculate the burn-through time is presented in Appendix B. The results from this experiment are listed in table 2. Because

Table 2. Summary of results from torsion pendulum experiment.

Incident energy (mJ)	Moment arm, s (cm)	Distance, l (cm)	Time, t_B (ps)
5 ± 1	2.12 ± 0.05	0.85 ± 0.20	86 ± 22
10 ± 1	1.63 ± 0.05	1.40 ± 0.20	92 ± 22
15 ± 1	1.45 ± 0.05	2.30 ± 0.20	117 ± 22

of the approximations made and the large number of factors necessary to perform this calculation, there is the possibility of large errors in the burn-through time. However, the results are in agreement with previous measurements of burn-through times for aluminum films[25,26,28,29]. These results indicate that the calculated burn-through time is on the same order as that estimated at the beginning of chapter 2. This confirmation of the 100 ps burn-through time indicates that most of the light reflected through the system consists of scattered light, light reflected from around the edges of the hole, and light reflected from the plasma. These burn-through times correspond to a path length of approximately 3 cm. However, the values obtained are at best an order of magnitude calculation.

Results

The attenuation was estimated at the beginning of the chapter to be at least a factor of 5000 for the double reflection experiment. That goal is achieved and even exceeded

for high incident energy levels. However, for low incident energy levels (less than 25 millijoules) attenuation is less than expected. As can be seen from figures 3.2, 3.4, and 3.5, the reflected energy is at its highest in the region corresponding to 15 - 30 millijoules of incident energy. There are several possible explanations for this result.

a) A plasma is created by the ablation of material at the focal spot. If the plasma does not move away from the surface with a sufficiently large velocity, light is reflected from it. The plasma created in this situation does not have a relatively high plasma temperature, however the plasma may still be reflective enough to account for the results obtained. Also, when an aluminum/mylar film undergoes laser ablation, the plasma moves along the surface laterally before expanding outward[30]. This creates a greater area for reflection of the pulse.

b) There is the possibility that light was reflected from the sides of the hole. Due to the small size of the hole created by the plasma, the return pulse may not be located at the same spot. The explosive process occurs after the plasma has left the surface of the mirror. It is caused by shock waves and heat conduction instigated by the ablation. Because this explosive process is slow, the material surrounding the focal spot may not have burned off when the light returns. This would allow light to be reflected from the edges of the hole.

c) The results from the experiments done at different distances between mirrors supports the assumption that the explosive process is slow. However, an examination of the relationship between damaged area and reflected energy, as depicted in figure 2.18,

indicates that this is not a significant factor with the purchased mirrors. The relationship between damaged area and reflected energy indicates that, as incident energy was increased, the damaged area is much greater and less light was reflected. Although the explosive damage process is slow, it can be hastened by various methods. A substitute for aluminum can be found, preferably one with a lower damage threshold and high reflectivity. Also, aluminum films with between 20 and 50 nm of gold deposited onto the aluminum have a much higher absorption of incident laser energy[23] than bare aluminum. Finally, the film mirror can be combined with another type of attenuator to limit the light transmitted through an optical system throughout the energy range of 15 to 30 mJ.

The double reflection experiment has shown to attenuate a laser pulse to a safe level except in the range of 15 to 30 mJ of incident light. Variations of this experiment can the results. However, the amount of reflected light in that energy range is as much as three times greater than the damage threshold. Another optical limiter, acting in tandem with the mirror system, can achieve the desired goal. An examination of one type of limiter is presented in chapters 4 and 5.

CHAPTER 4

NON-LINEAR ABSORPTION MECHANISMS

Background

Another type of passive optical limiter is a non-linear absorbing liquid. The non-linear characteristics are necessary to produce high levels of attenuation. In order for a substance to be a non-linear absorber, it must behave contrary to the Beer-Lambert Law. Such materials have complicated absorption mechanisms. Two possible absorption mechanisms are presented in this chapter.

Semi-Limiting Mechanism

A multi-photon absorption mechanism has been derived to explain the limiting characteristics of chloro-aluminum phthalocyanine (CAP), a laser dye, which exhibits this limiting characteristic[31]. This scheme is illustrated in figure 4.1. The physical description

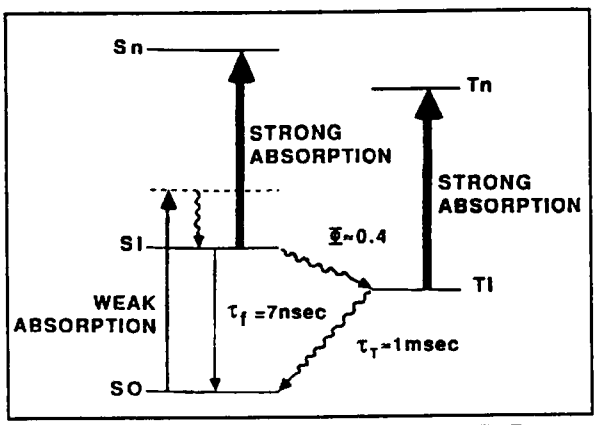

Figure 4.1. Absorption scheme for CAP.

of this multiphoton absorption scheme is based on the weak absorption of a single photon by a molecule. From this excited state, the molecule quickly decays and then absorbs another photon (strong absorption). Mathematically, this scheme can be described in the follwing manner:

$$n_0 = n_0' \exp(-\sigma_0 F t)$$

where n_0' is the inital population density at the ground state, σ_0 is the excited state cross section, F is the photon energy, and t is the decay time. Then,

$$\frac{dn_0}{dt} = -\sigma_0 F n_0 .$$

Letting n_1 be the number of atoms populating the second state and σ_1 be the cross section of the second excited state, then

$$\frac{dn_1}{dt} = \sigma_0 F n_0' \exp(-\sigma_0 F t) - \sigma_1 F n_1 . \qquad (4-1)$$

Equation 3-1 can be written in terms of the change in total photon energy during the travel through the medium.

$$\frac{dF}{dt} = -n_0 \sigma_0 F - \frac{F t \sigma_0 n_0' [\exp(-\sigma_0 F t) - \exp(-\sigma_1 F t)]}{\sigma_0 - \sigma_1} .$$

This can also be expressed as:

$$C\,dl = dF \{ F [\exp(-\sigma_0 t_0 F) - \exp(-\sigma_1 t_1 F)] \}^{-1} \qquad (4-2)$$

where C is a constant of proportionality. The equation was solved numerically and the result graphed in figure 4.2, indicates a semi-limiting behavior.

Limiting Mechanism

Another absorption mechanism has been proposed[32]. This scheme indicates

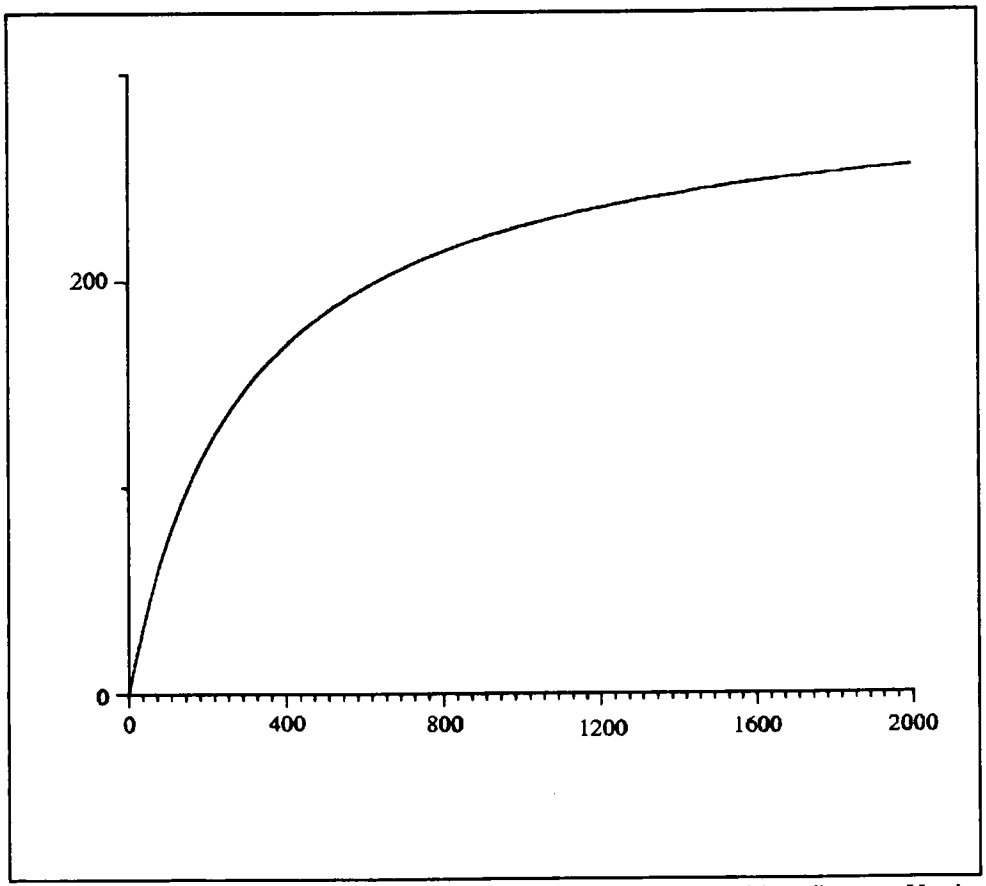

Figure 4.2. Theoretical plot of equation 4-2. Horizontal axis is incident fluence. Vertical axis is transmitted fluence in J/cm^2

that the initial molecule is disassociated during the absorption of two photons, and one or both of the resulting fragments are single-photon absorbers. Letting **M** be such a molecule, then:

$$\mathbf{M} + 2\hbar\omega \rightarrow \mathbf{M}_1 + \mathbf{M}_2 \qquad \text{(two photon absorption)}$$

$$\mathbf{M}_1 + \hbar\omega \rightarrow \mathbf{M}_1^* \qquad \text{(one photon absorption)}$$

$$\mathbf{M}_1^* + \mathbf{M}' \rightarrow \mathbf{M}_1 + \mathbf{M}' \text{ (excited)}$$

The quenching of the excited state by collision with another species is a fast process. The emmission of an additional photon in a random direction is a slow process.

This absorption process can be written mathematically as:[32]

$$\frac{\partial \Phi}{\partial z} = \frac{-3\beta\Phi^2}{2\pi d^2(1 + 4z^2/b^2)} \qquad (4 - 3)$$

where: z = length of the medium = 0.1cm,

β = absorption coefficient $\approx$ 1 x 10^{-5} cm/Watt,

$b = F\lambda/\pi d_0$,

F = focal lenght of the lens = 10 cm,

λ = wavelength of laser = 532 nm,

d_0 = diameter of laser beam incident on the lens = 0.6 cm,

$d = F\lambda/\pi d_0$, and

Φ = laser energy per pulse.

When equation 4-3 is integrated and the aforementioned constants are inserted, the result are as graphed in figure 4.3. This indicates that it is possible for this scheme to work as long

as the absorption coefficient, ß, is large enough.

Summary

Ideally, the limiting mechanism shown in figure 4.3 is the desired goal for an optical limiter. The experiments explained in chapter 5 were conducted to determine the absorption of several different organometallic dyes (phthalocyanines). The results of those experiments should indicate which mechanism presented here is applicable.

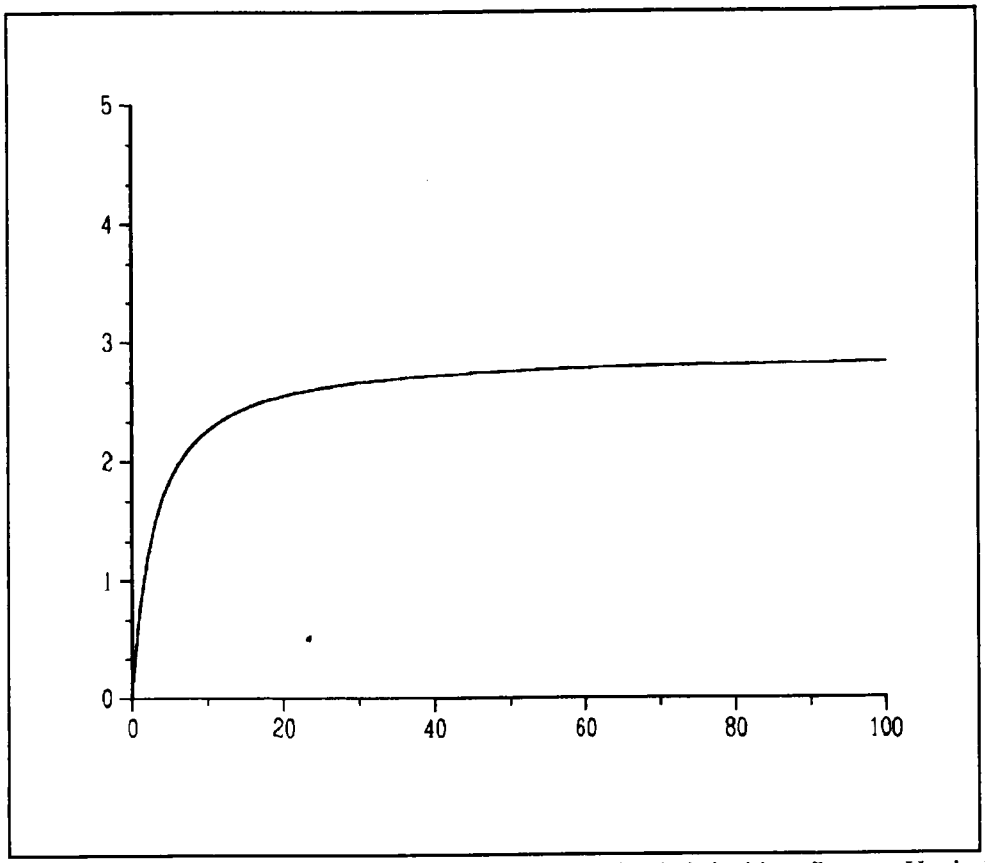

Figure 4.3. Theoretical plot of equation 4-3. Horizontal axis it incident fluence. Vertical axis is transmitted fluence in J/cm^2.

CHAPTER 5

METALLIC PHTHALOCYANINES

Background

Metallic phthalocyanines (pcs) are organo-metallic compounds that were first synthesized in 1907. Presently, they are used in a wide variety of products, such as paints, plastics, printing inks, crayons, food coloring, and laser dyes[33]. A copper phthalocyanine molecule is shown in figure 5.1. Recently, chloro-aluminum phthalocyanine (CAP) was found to have optical limiting characteristics[31,34,35]. Optical limiting has been investigated in other organo-metallic compounds, primarily indanthrone[36] and fullerene[37].

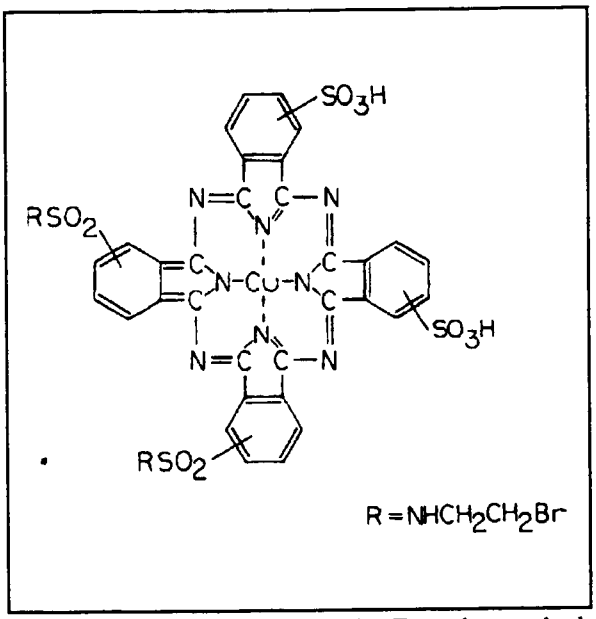

Figure 5.1. Copper pcs molecule. For other pcs', the copper atom is replaced with another metal atom.

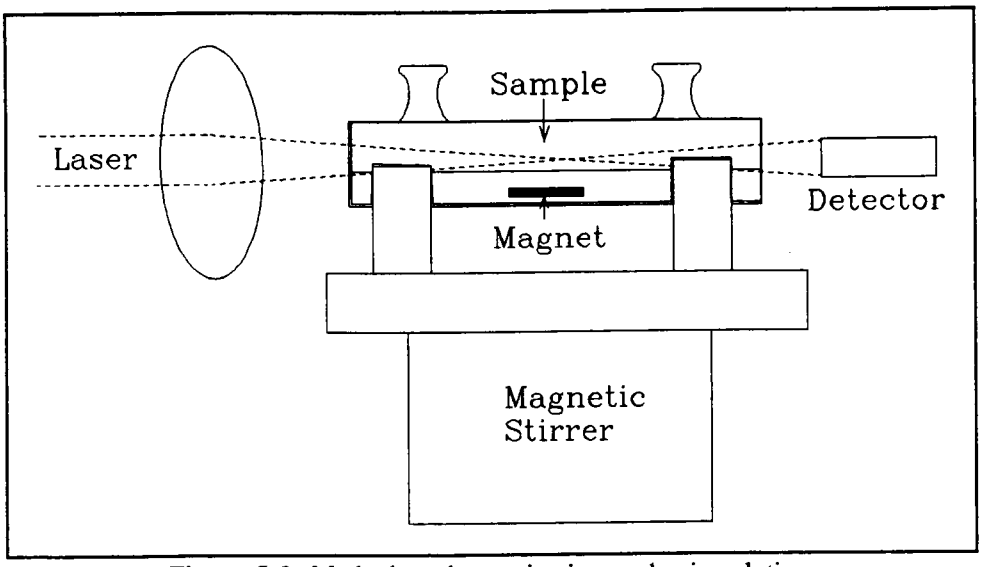

Figure 5.3. Method used to maintain pcs dye in solution.

runs. The transmitted light is measured upon exiting the cell by either a photodiode connected to a sample and hold unit or by a Gentec joulemeter. The normal transmission of each sample is measured by a Cary photospectrometer. The preparation of the phthalocyanine (pcs) solutions is explained in appendix C.

Results

The combined results for the greater molalities of each substance tested at 482 nm are shown in figure 5.4. As indicated in the graph, all five dyes exhibit limiting characteristics. However, since each dye has a different transmission at each wavelength, their overall limiting behavior throughout the visible region must be examined individually. Explanations of results for each type of phthalocyanine are detailed in appendices D through H. Sodium phthalocyanine performs best at 532 and 640 nm. Zinc pcs performs best at 630 and 660 nm. Plain pcs performs best at 482 nm. CAP

Experiment

The limiting characteristics of five different phthalocyanines are measured. The schematic for this experiment is detailed in figure 5.2. A dye chamber was installed to test the solutions at various wavelengths. For the wavelengths of 585, 630, 640, and 660 nm, the pump beam is 532 nm. For the 482 nm wavelength, the pump beam is 355 nm. After passing through the dye chamber, the laser pulse is split with a glass plate to monitor the incident power. The rest of the pulse passes through neutral density filter(s) to attenuate the pulse to different power levels. The pulse is then either passed directly through the sample cell without focussing, or it is focussed at the center of the cell with a 10 cm focal length lens. Because the dye tends to separate from the ethanol when sitting for a period of time, a magnet is placed in the cell, which is mounted over a magnetic stirrer (figure 5.3). This insures that the dye remains in solution during the data

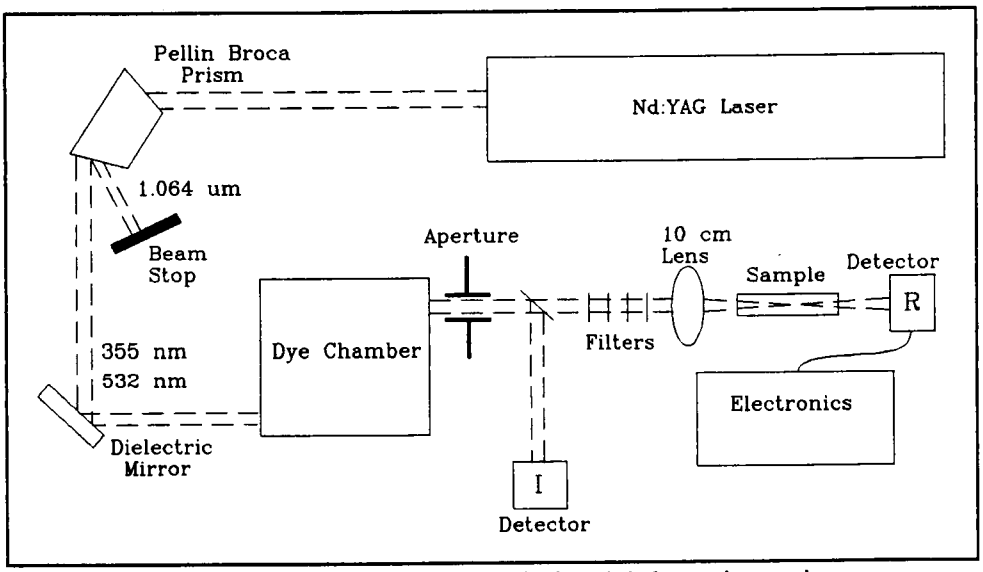

Figure 5.2. Experimental schematic for phthalocyanine testing.

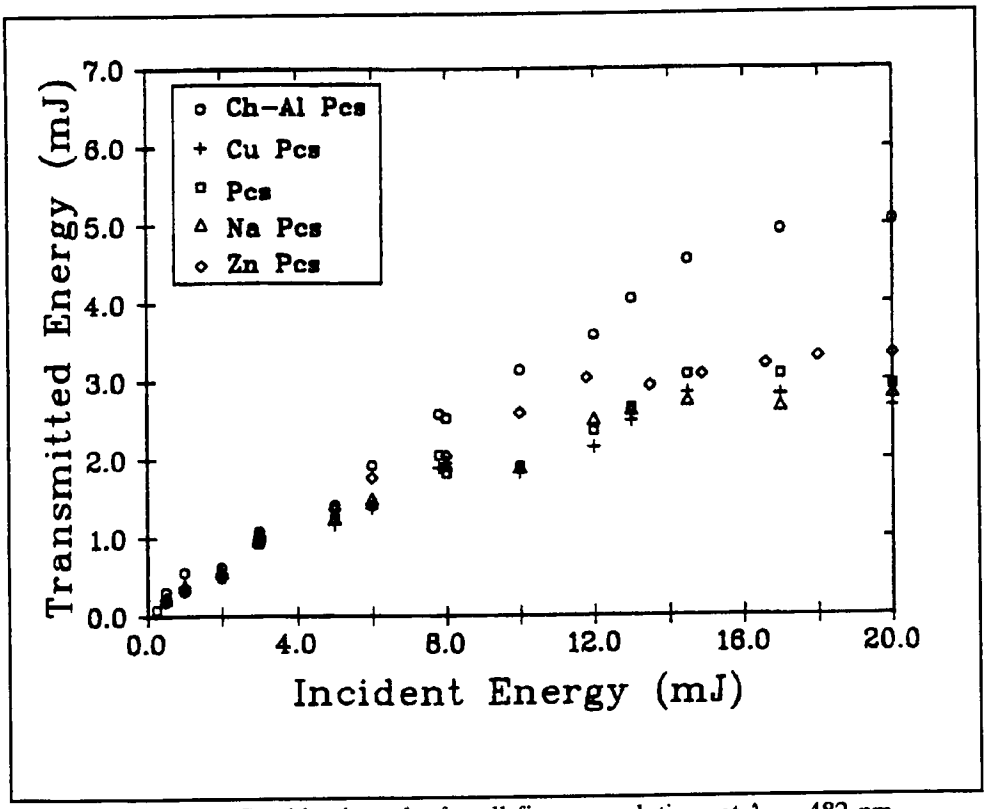

Figure 5.4. Combined results for all five pcs solutions at λ = 482 nm.

and copper pcs performed for the most part as linear absorbers.

Several typical results are pictured in figures 5.5 - 5.7. The lines in figures 5.5 - 5.7 indicate the normal transmission of light measured by the photospectrometer. The results in figures 5.5 and 5.6 indicate a large degree of optical limiting. As can be seen, there is absorption both in the focussed and the unfocussed situation, which is necessary for a multiphoton absorption process. In figure 5.7, the absorption in the unfocussed state is nearly the same as the normal transmission. This indicates that any attenuation of the beam in the focussed state is due either to optical breakdown or the absorption cross section is very small.

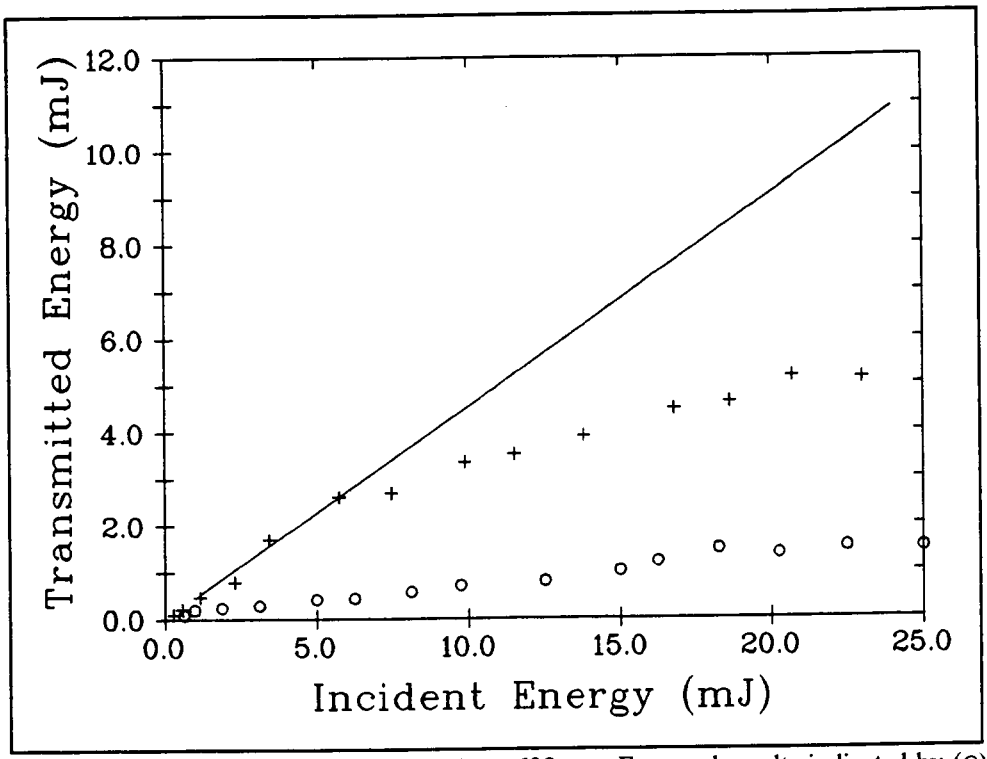

Figure 5.5. Transmission of zinc pcs at λ = 630 nm. Focussed results indicated by (○) and unfocussed results by (+).

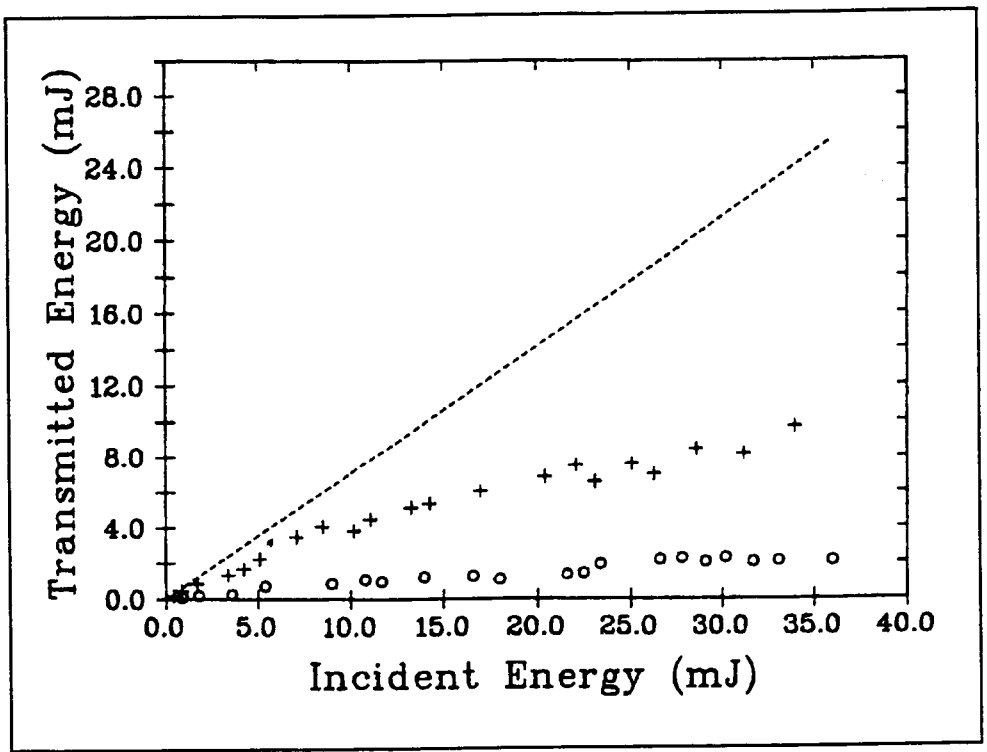

Figure 5.6. Transmission of sodium pcs at λ = 585 nm. Focussed results indicated by (○) and unfocussed results by (+).

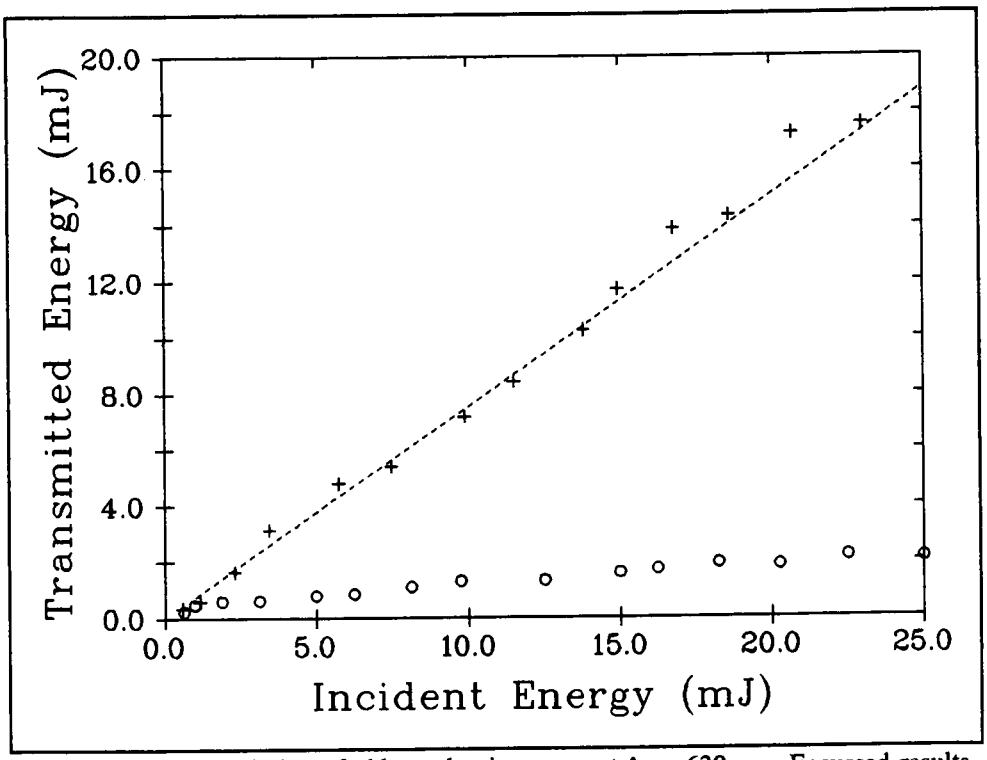

Figure 5.7. Transmission of chloro-aluminum pcs at λ = 630 nm. Focussed results indicated by (o) and unfocussed results by (+).

Figures 5.8 and 5.9 show the attenuation of zinc pcs at 630 nm. The focussed case shown in figure 5.8 indicates an attenuation factor becoming constant at higher energies. This attenuation factor levels off at approximately 40. The attenuation for the unfocussed situation in figure 5.9 shows that the liquid, at the lower energy densities, behaves as a linear absorber would.

By themselves, the metal phthalocyanines cannot attenuate the incident light to the desired level without being in such high concentration as to render the liquid opaque. However, in combination with thin film mirrors, desired attenuation can be attained. For example, the attenuation depicted in figure 5.9 is approximately a factor of 10 for an incident energy of 25 mJ. Combined with the results of the double-reflection mirror system (figure 3.2), the transmission of light through the system will be, at the most,

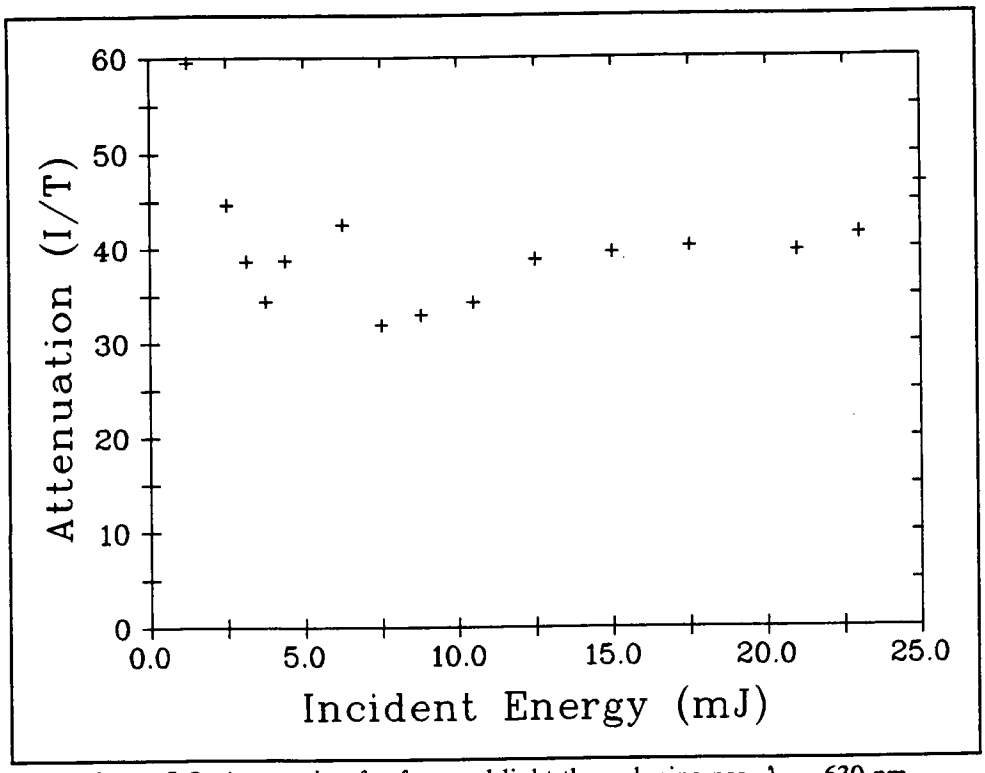

Figure 5.8. Attenuation for focussed light through zinc pcs. λ = 630 nm.

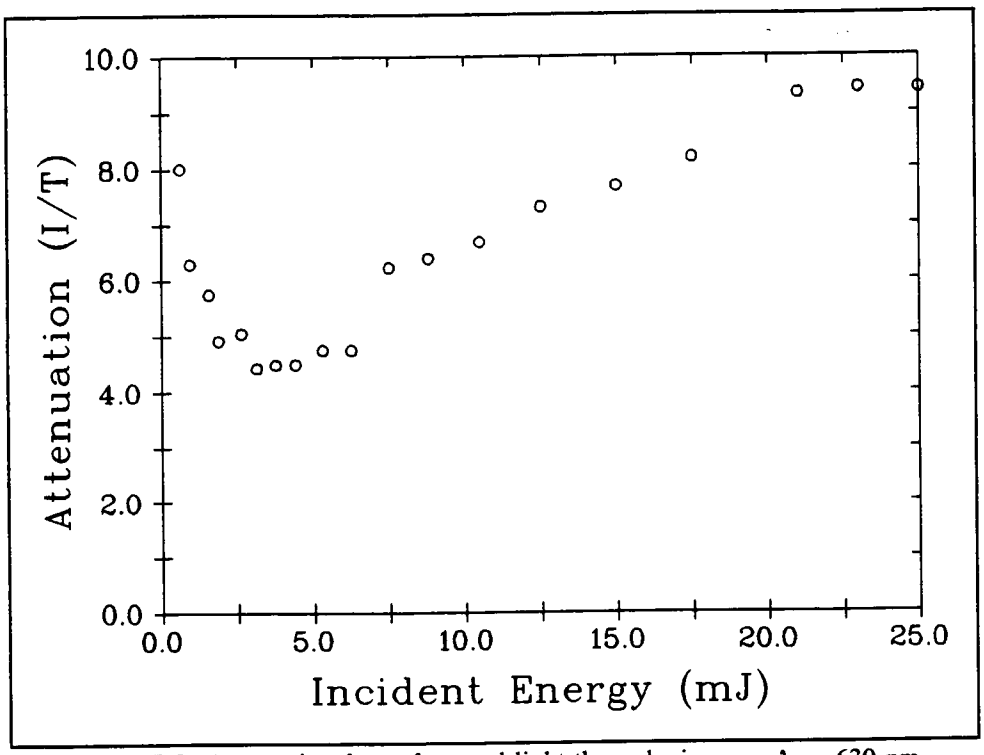

Figure 5.9. Attenuation for unfocussed light through zinc pcs. λ = 630 nm.

3.1 μJ. Two possible combinations are shown in figure 5.10. In figure 5.10.a, the light is focussed at the surface of the mirror, which is immersed in the pcs solution. The advantage with the first configuration is that there will be a high power density in the solution at the surface of the mirror, allowing the pcs to attenuate the light by a factor of 25 to 50. Unfortunately, a large enough cell to hold the mirrors was not available at the time the experiments were conducted. Therefore, only the experiment shown in figure 5.10.b was conducted. The equipment used was the same as that in figure 2.4, the only difference being that a cell with sodium pcs was placed in the beam path before the beam splitter. The results of this trial are graphed in figure 5.11, along with results of the same experiment conducted without the presence of the sodium pcs cell. The mirror was destroyed when 1 millijoule was focussed onto it, so that higher energy data is not available. However, it is clear that the attenuation is significantly improved at lower energies; by a factor of 2 at I = 0.5 mJ.

The results of the pcs experiments do not reveal which limiting scheme presented in chapter 4 is applicable. However, there is marked optical limiting in the majority of both focussed and unfocussed trials. The combination with the mirrors indicates that attenuation of the laser pulse to below the damage threshold of 10 μJ is possible.

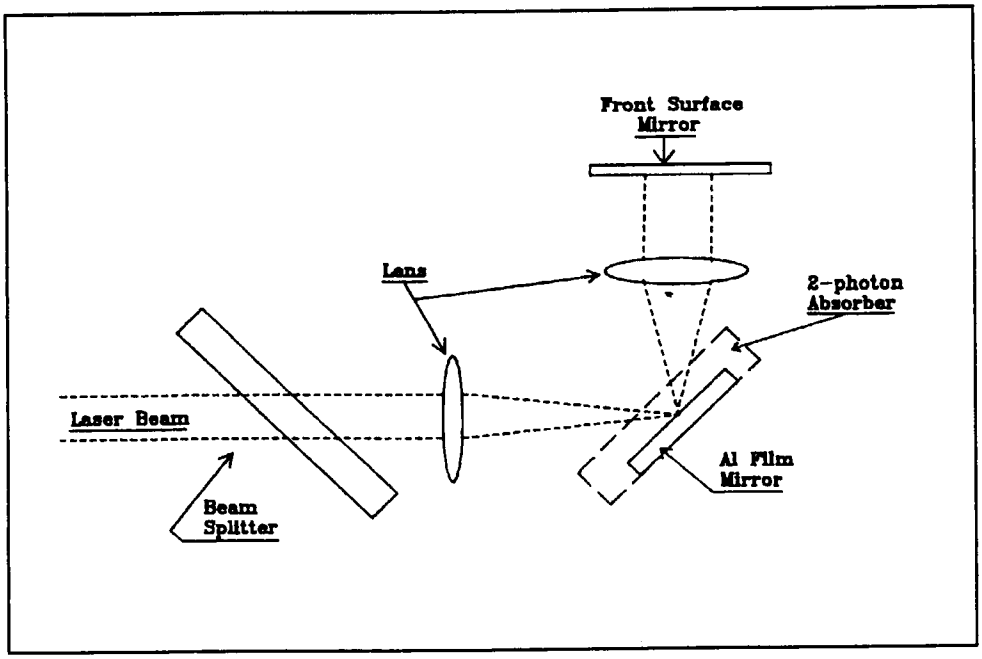

a)

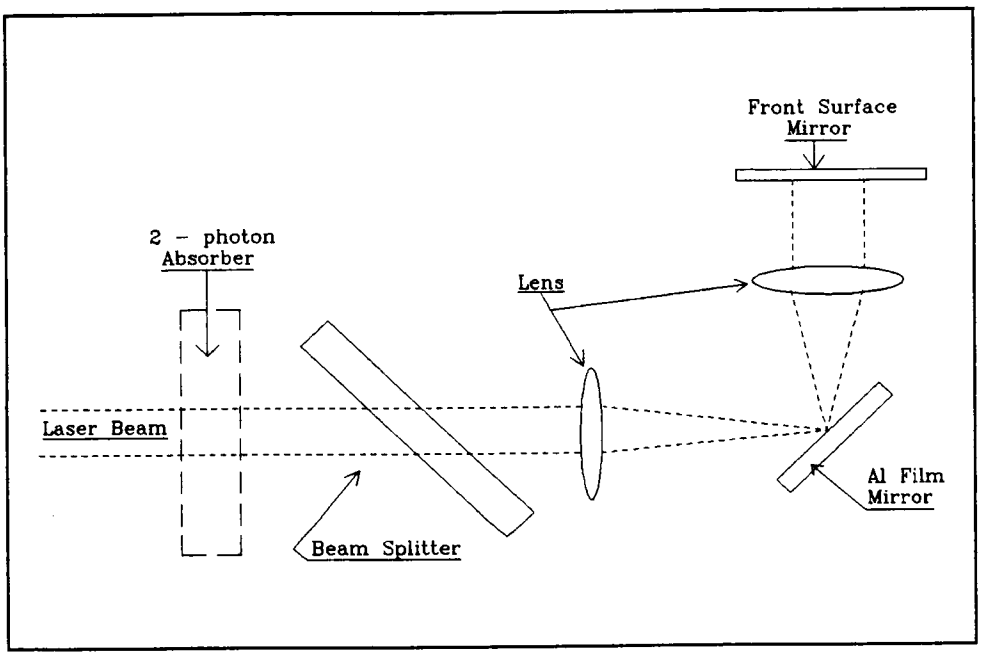

b)

Figure 5.10. Two schemes for incorporating pcs and thin film mirror.

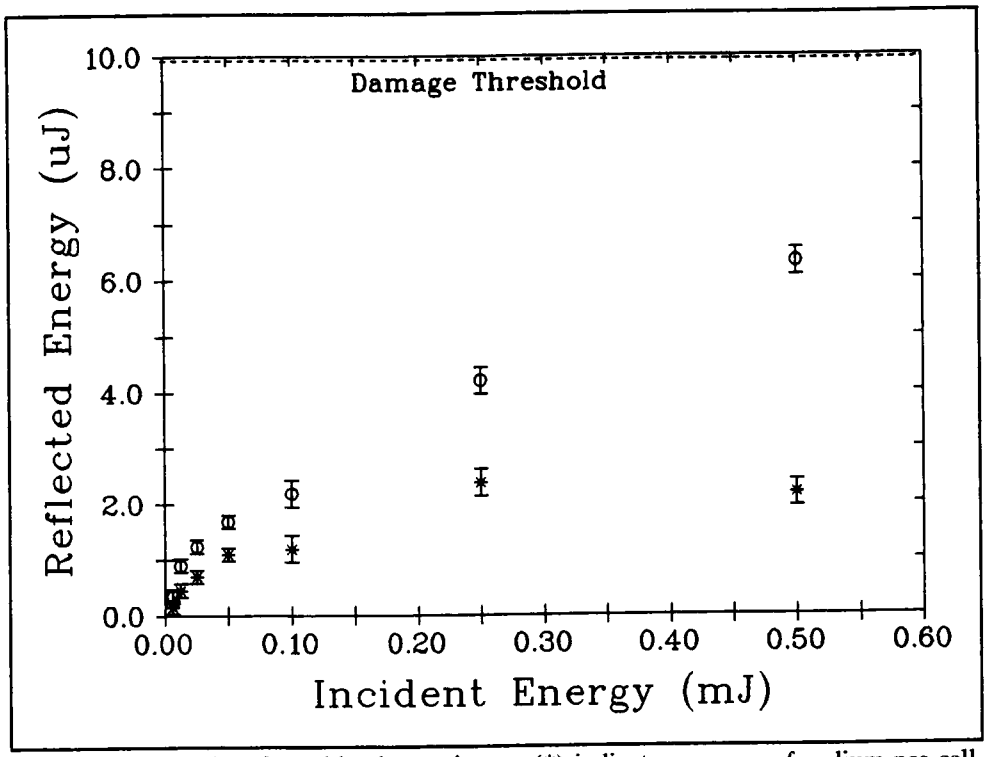

Figure 5.11. Results of combined experiment. (*) indicate presence of sodium pcs cell. (○) indicates absence of sodium pcs.

CHAPTER 6

UNCERTAINTIES

Mirror Experiments

The requirement to focus the laser pulse at the surface of the mirror with the smallest spot size possible produced the most important uncertainty in these experiments. A striking example of this is that the purchased mirrors can be destroyed with a single shot at 1 millijoule of laser energy during one trial and not be destroyed in another trial until 35 millijoules was focussed on the mirror. This variation, however, is more important when actual optical design is done than for determining the validity of experimental results. With the supposed worst focussing situation, the results obtained still met the criteria established except for the range of 20-30 millijoules of incident energy.

The collection of data is another source of uncertainty. Some reflected energies were measured with the Gentek joulemeter connected to an oscilliscope instead of the computer. This could introduce errors in the amount of voltage recorded by as much as 25% for the lowest setting on the voltage scale of the oscilliscope, however, as the signal became larger, the error in reading the voltage compared to the actual voltage becomes small.

The laser energy can be a significant source of uncertainty because the laser is not mode-locked and the energy from shot to shot can vary as much as 5%. This is an acute problem when trying to work with single shots, because the laser is designed to run at

10 Hz and at full output energy which is 450 millijoules per pulse. The laser can be operated at full power and the beam can be attenuated by using filters, however, when the repitition rate is not 10 Hz, the Q-switch trigger tends to drift. This means that the Q-switch can be out of optimum sychronization with the lamp and the pulse energy will decrease. Also, not firing at 10 Hz causes the doubling crystal to be at a temperature which is much lower than is optimal.

Another uncertainty was the presence of ASE (amplified spontaneous emission), which was minimized by passing the beam through an aperture. There is also a slight non-linear response of the photodiode. There was damage present in the optical elements; the dielectric mirror was slightly burned, the pellin-broca prism had slight damage, and most of the lenses that were used had some damage streaks. The Gentek joulemeter had a non-uniform response; there was a spatial variation in the sensitivity of the meter. This was minimized by moving the meter until the maximum scale reading was obtained and then marking that spot on the meter. The meter was rarely moved until the next experiment, when the laser pulse would be returned to that marked spot.

The variation of results from actual values could not have been more than 15 to 20%. The significance of the uncertainties to the results must be compared with the desired goals. The light had to be attenuated to at least 5-10 μJ. For the greatest reflected light with the purchased mirrors, which was 31 μJ, even a 50% variation would not bring it below the required level.

Phthalocyanine Experiment

The uncertainties present in these experiments are primarily due to the variation in laser power. Uncertainties due to data collection, photodiode response, spatial dependence of the Gentek joulemeter, and damage to optical elements are the same as with the mirror experiments. The variation in the laser power is not due to the operation of the YAG, since it was operated at full power and at 10 HZ, but with the dye chamber. The laser dyes have a useful lifetime, after which they will decay and their conversion efficiency decreases rapidly. The dyes will decay after being exposed for a period of time with the laser firing at 10 Hz. For the longer wavelength dyes, this decay is very slow, however for the blue dyes the decay is rather fast. This necessitated changing the blue dye halfway through the experiment. The tendency for the dye to decay was known from the outset. To prolong the dye lifetime, the laser pulse was blocked before entering the dye chamber when data was not being taken.

CHAPTER 7

CONCLUSION

The goal of these experiments was to find a method to limit the intensity of a laser pulse emerging from an optical system to below that level at which eye damage occurs. The results obtained for the aluminum mirrors and for the phthalocyanine compounds do not meet that goal individually. However, if their use is combined in an optical system, it is likely that the goal will be achieved. The only remaining experiment to perform is to place a mirror into a cell containing a phthalocyanine compound and subjecting that cell to laser energies between 15 and 30 millijoules. A piece of aluminum film from a destroyed mirror was placed in a solution of sodium pcs for two months. No degredation of the film was observed after that time. This indicates that the mirror/pcs combination is chemically stable, and transmission of normal light would not be seriously affected by the combination.

A schematic of a possible optical design is presented in figure 7.1. Laser-safe binoculars have been designed (figure 7.2) and patent apllications have been filed.

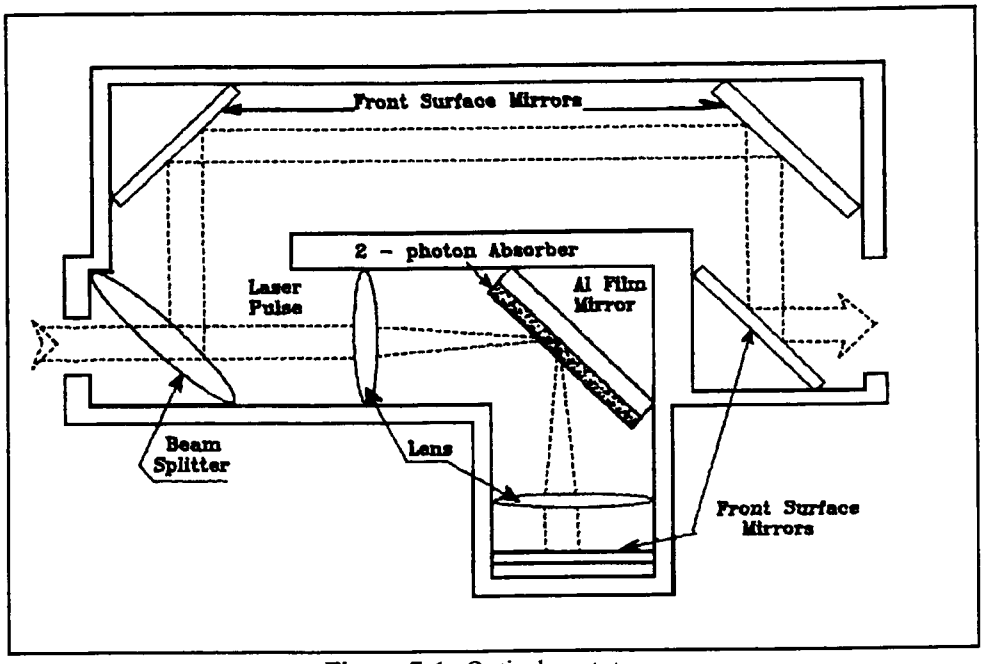

Figure 7.1. Optical prototype.

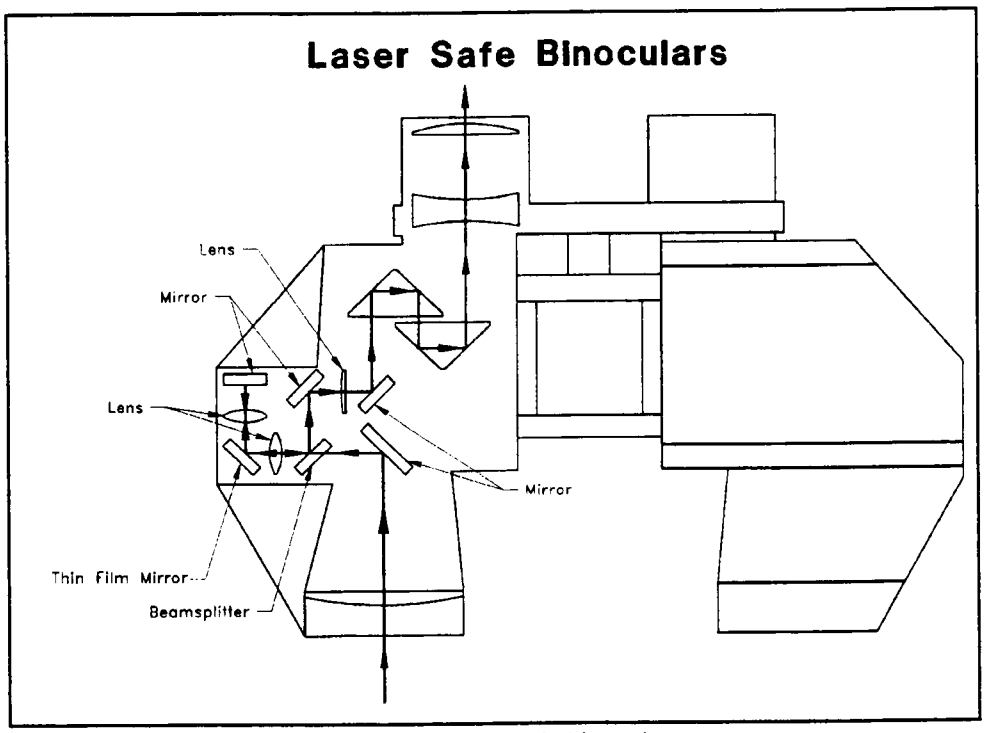

Figure 7.2. Laser-safe binoculars.

LIST OF REFERENCES

List of References

1. J. Grossman, "Military Laser Systems: A Costly Search For Ultimate Weapons," Photonics Spectra, pp. 84-90, July 1991.

2. J. Taboada, R.W. Ebbers, "Ocular Tissue Damage Due to Ultrashort 1060 nm Light Pulses From a Mode-locked Nd:Glass Laser," Appl. Opt. **14** (8), pp. 1759-1781 (1975).

3. J. Taboada, W.D. Gibbons, "Retinal Tissue Damage Induced by Single Ultrashort 1060 nm Laser Light Pulses," Appl. Opt. **17** (18), pp. 2871-2873 (1978).

4. D. Sliney & M. Wolbarsht, *Safety with Lasers and Other Optical Sources*, pp. 116-143, Plenum Press, New York (1980).

5. A.P. Bruckner, J.M. Schurr, and E.L. Chang, "Biological Damage Threshold Induced by Ultrashort Fundamental, 2nd, and 4th Harmonic Light Pulses From a Mode-Locked Nd:Glass Laser," USAF School of Aerospace Medicine Report SAM-TR-80-47, pp. 46-58, Brooks AFB, TX (1980).

6. A.P. Bruckner and J. Taboada, "Retinal Tissue Damage Induced by 6-psec 530 nm Laser Light Pulses," Appl. Opt. **21** (3), pp. 365-367 (1982).

7. W.D. Gibbons, "Retinal Burn Thresholds for Exposure to a Frequency-Doubled Neodymium Laser," USAF School of Aerospace Medicine Report SAM-TR-73-45, pp. 8-13, Brooks AFB, TX (1973).

8. W.T.Ham, H.A. Mueller, J.J. Ruffolo, R.K. Guerry, A.M. Clarke, "Ocular Effects of GaAs Lasers and Near Infrared Detectors," Appl. Opt. **23** (13), pp. 2181-2186 (1984).

9. G. Laufer, "Primary and Secondary Damage to Biological Tissue Induced by Laser Radiation," Appl. Opt. **22** (5), pp. 676-681 (1983).

10. R.R. Reed, J. Taboada, and G.A. Greiss, "Thresholds and Mechanisms of Retinal Damage From a White-Light Laser," Health Phys. **39**, pp. 33-39 (1980).

11. W.D. Gibbons and R.G. Allen, "Retinal Damage From Suprathreshold Q-Switch Laser Exposure," Health Phys. **35**, pp. 461-469 (1978).

12. J.F. Ready, *Effects of High Power Laser Radiation*, pp. 317-332, Academic Press, New York (1971).

13. A.J. Welch and G.D. Polhamus, "Measurement and Prediction of Thermal Injury in the Retina of the Rhesus Monkey," IEEE Trans. Biomed. Eng., **BME-31** (10), pp. 633-644 (1984).

14. R.G. Allen, S.J. Thomas, J.A. Zuclich, and M.A. Blankenstein, "Ocular Effects of Pulsed Nd Laser Radiation: Variation of Threshold With Pulsewidth," Health Phys. **49** (5), pp. 685-692 (1985).

15. ANSI, Z 136.1 - 1986, "American National Standard for the Safe Use of Lasers," American National Standards Institute, pp. 66-79 New York (1986).

16. I.C. Khoo and Y.R. Shen, "Liquid Crystals: Nonlinear Optical Properties and Processes," Opt. Eng. **24** (4), pp. 579-586 (1985).

17. S.K. Lo, S.A. Jenekhe, S.T. Wellinghoff, and D.K. Greenlaw, Technical Report, NATICK/TR-861057L, "Eye Protection Against Tunable Lasers," pp. 5-30 (1986).

18. C.T. Seaton, "Nonlinear Guided Wave Applications," Opt. Eng. 24 (4), pp. 593-602 (1985).

19. G.M. Carter, Y.J. Shen, and S.K. Tripathy, "Third-Order Nonlinear Susceptibility in Multilayers of Polydiacetylene," Amer. Chem. Soc. Symp. 233, pp. 213-228 (1982).

20. E.W. van Stryland, Y.Y. Wu, D.J. Hagan, M.J. Soileau, and K. Mansour, "Optical Limiting With Semiconductors," J. Opt. Soc. Amer. B 5, pp. 1980-1989 (1988).

21. Z.G. Sztankay, R.J. Wellman, D. McGuire, "Evaluation of a Limiting Mirror For Laser Eye and Sensor Protection," US ARMY MACOM Report HDL-TR-1683 (1975).

22. H. Buhay, R.Q. Moy, N.P. Muraka. "Sacrificial Filter," US ARMY Tank-Automotive Command Report 12903 (1983).

23. W. Mroz, R. Arendzikowski, S. Denus, J. Farny, H. Fiedorowicz, K. Jeziak, M. Mamczur, S. Nagraba, W. Pawlowicz, A. Wilczynski, J. Wolowski, P. Bitzan, L. Driska, J. Limpouch, G. Loncar, L. Pina, and J. Vondrasek, "Energy Transport Through Thin Aluminum Foils in Laser-Target Experiment," Laser and Particle Beams 7 (1), pp. 3-14 (1989).

24. M.H. Key, W.T. Toner, T.J. Goldsack, J.D. Kilkenny, S.A. Veats, P.F. Cunningham, and C.S. Lewis, "A Study of Ablation by Laser Irradiation of Plane Targets at Wavelengths 1.05, 0.53, and 0.35 μm," Phys. Fluids. **26** (7), pp. 2011-2026 (1983).

25. B. Arad, S. Eliezer, S Jackel, A Krumbein, H.M. Loebenstein, D. Salzmann, A. Zigler, H. Zmora, and S. Zweigenbaum, "Effects of Pulse Duration and Polarization on Momentum and Energy Transfer to Laser-Irradiated Targets," Phys. Rev. Let. **44** (3), pp. 326-329 (1980).

26. M.A. Gusinow, J.P. Anthes, and M.K. Matzen, "Measurements of the Ion-Expansion Structure and Velocities from Thin-Foil Laser-Target Interactions," App. Phys. Let. **33** (9), pp. 800-802 (1978).

27. D. Halliday and R. Resnick, *Fundamentals of Physics, 2nd Edition*, pp. 811-812, John Wiley & Sons, New York (1986).

28. B. Arad, S. Eliezer, Y. Gazit, H.M. Loebenstein, A. Zigler, H. Zmora, and S. Zweigenbaum, "Burn-through of Thin Aluminum Foils by Laser-Driven Ablation," J. Appl. Phys. **50** (11), pp. 6817-6821 (1979).

29. J. Grun and B.H. Ripin, "Ballistic Pendula for Measuring the Momentum of a Laser-Produced Plasma," Naval Research Laboratory Memorandum Report 4900, NRL, Washington, D.C. (1982).

30. A. Zigler, H. Zmora, Y. Paiss, and J.L. Schwab, "The Expansion of a Laser-Produced Aluminum Plasma and the Heat Penetration in Multi-Layered Targets," J.Phys D. **10**, pp. L159-L162 (1977).

31. D.R. Coulter, V.M. Miskowski, J.W. Perry, T.H. Wei, E.W. van Stryland, and D.J. Hagan, "Optical Limiting in Solutions of Metallo-Phthalocyanines and Naphthalocyanines," SPIE **1105**, *Materials for Optical Switches, Isolators, and Limiters*, pp. 42-51 (1989).

32. M.G. Payne, C.H. Chen, W.R. Garrett, and D. Templeton, "High Intensity Laser Beam Attenuation Based on Two-Step Absorption Mechanism," submitted to J. of Appl. Phys.

33. F.H. Moser and A.L. Thomas, *The Phthalocyanines, Vol. I Properties*, pp.184-192 CRC Press, Boca Raton, Florida (1983).

34. M.J. Solieau, T.H. Wei, M. Sheik-Bahae, D.J. Hagan, M. Sence, and E.W. van Stryland, "Nonlinear Optical Characterization of Organic Materials," Mol. Pdf. Cryst., **207**, pp. 97-101 (1991).

35. L.W. Tutt and S.W. McCahon, "Reverse Saturable Absorption in Metal Cluster Compounds," Opt. Let. **15** (12), pp. 700-702 (1990).

36. R.C. Hoffman, K.A. Stetyick, and R.S. Potember, "Reverse Saturable Absorbers: Indanthrone and its Derivatives," J. Opt. Soc. Am. B **6** (4), pp. 772-777 (1989).

37. L.W. Tutt and A. Kost, "Optical Limiting Performance of C_{60} and C_{70} Solutions," Nature **356**, pp. 225-226 (1991).

APPENDICES

APPENDIX A

CALCULATION OF DAMAGE THRESHOLD

The damage threshold of the purchased aluminum mirrors is an important consideration. If the damage threshold of the mirror is greater than that of the eye, it is not a useful device. The theoretical equation for calculating this has been derived elsewhere[22]. It is:

$$u = D\rho \{ C_s T_m + L_m + C_l (T_v - T_m) + L_v \} [(1 - r)(1 - \Lambda)]^{-1},$$

where u = irradiance,

D = thickness of the metal film = 500 Å,

C_s = the solid heat capacity = 4.94 cal/gC°,

C_l = the liquid heat capacity = 7.0 cal/gC°,

L_m = the heat of transition for melting = 2.57×10^3 cal/g,

L_v = the heat of transition for vaporization = 67.9×10^3 cal/g, and

ρ = density of aluminum = 2.698 g/cm³.

The resulting irradiance is:

$u = 1.19$ J/cm³.

Multiplying this by the smallest damaged area visible in the microscope,

E = energy = $u [\pi (0.4 \times 10^{-3})^2]$

$= 0.299$ μJ.

The incident energy was 0.13 μJ, so this equation provides a good approximation of the damage threshold.

APPENDIX B

DERIVATION OF t_B

When the laser pulse is incident on the mirror, part of it is reflected and the rest is absorbed in the film. Let the total amount of reflected energy be R_T. Then,

$$R_T = R_1 + R_2.$$

R_1 is the light reflected from t = 0 to t_B, where t_B is the burn-through time. R_2 is the light reflected from t_B to t_p, where t_p is the pulse length of the laser.

R_2 is the light reflected from the edges of the hole + scattered light + light reflected by plasma. Assuming the contribution to R_T by R_2 is small compared to R_1, then

$$R_T \approx R_1.$$

During the time from t = 0 to t_B, assume that the reflectance, Λ, of the mirror does not change significantly until the hole is definately formed at t_B, so that the energy absorbed by the mirror during that time can be expressed as:

$$E_{abs} = E_T - R_T.$$

$$= R_T/\Lambda - R_T.$$

$$= R_T (1/\Lambda - 1).$$

Now, assuming that this energy provides the rotation to the pendulum, then

$$E_{abs} = \text{Rotational Kinetic Energy}$$

$$= \tfrac{1}{2} I\omega^2$$

$$= \tfrac{1}{2} I(\theta/t_B)^2.$$

so that

$$t_B = \theta\, [(mR^2)/(4E_{abs})]^{1/2}.$$

With R = 3.1 cm,

m = density/volume,

volume = π[(focal length)(beam divergence)½]^2(film thickness),

focal length = 5 cm,

beam divergence = 0.5 mrad,

film thickness = 500 Å, and

Λ = 0.95,

the burn time can be calculated with the data in table 2 of chapter 3.

APPENDIX C

PHTHALOCYANINE SAMPLE PREPARATION

Each phthalocyanine dye is dissolved in pyridine and then drops of that solution are dissolved in ethanol. The respective weights of the pyridine and the pcs powder were recorded. The weight of the ethanol is recorded before and after the pyridine/pcs mixture was added. The molality of each compound is then calculated by the following method.

M_{Pcs} = mass of the phthalocycanine powder,

M_p = mass of pyridine,

M_m = the mass of the amount of pyridine-pcs mixture added to the ethanol,

M_e = the mass of the ethanol,

M_{PcsE} = the mass of the Pcs powder in the ethanol,

V = the volume of the ethanol,

d = the density of the ethanol, and

MW = the molecular weight of the pcs powder.

$$M_{PcsE} = \frac{M_{Pcs}\, M_m}{MW\,(M_p + M_{Pcs})} \qquad (C - 1)$$

The volume of the ethanol is the mass divided by the density

$$V = M_e/d.$$

This is used to find the molality of the solution, which is the concentration expressed in terms of moles/liter.

$$\text{Molality} = \frac{M_{PcsE}\,(1000\ cm^3/l \div V)}{(1000\ cm^3/l \div V)} \qquad (C - 2)$$

The measured masses are shown in table 3 and the molalities of each sample are listed in table 4.

Table 3. Masses used to calculate Pcs molalities. The masses were measured with a Mettler AE260 electronic scale.

	M_{Pcs} (g)	M_p (g)	M_m (g)	M_c (g)
Chlorol-Aluminum	.0275	50.8337	.0435 .3055	47.223 50.0481
Copper	.0241	49.0789	.0520 .2619	49.993 47.1997
Pcs	.0361	61.2050	.0757 .2524	50.0855 48.3007
Sodium	.0304	44.9781	.0599 .2327	48.5059 49.3290
Zinc	.0262	45.5772	.0309 .1060	22.3140 22.9971

Table 4. Molalities of Phthalocyanine - Pyridine - Ethanol solutions.

	Chloro-Aluminum	Copper	Plain	Sodium	Zinc
Solution 1 Molality (x 10^{-6})	0.68	0.70	1.37	1.18	1.09
Solution 2 Molality (x 10^{-6})	4.43	3.73	4.51	4.50	3.60

APPENDIX D

CHLORO-ALUMINUM PHTHALOCYANINE

The transmission for CAP throughout the visible spectrum for both concentrations is shown in figure D.1. The experimental results are shown in figures D.2 through D.7. For the smaller wavelengths, the graphs show that the absorption coefficient is relatively small, as the unfocussed transmission is nearly linear. For the longer wavelengths, the absorption is a single photon absorption[28]. The general trend for all of the pcs data shows that more light is absorbed when focussed than unfocussed*. This is a strong indication that the absorption process is power-dependent, which is a strong indication that the absorption scheme described by equation 3.3 is applicable in this case. For all transmission graphs at individual wavelengths, focussed results are symbolized by a (+) and unfocussed results are symbolized by a (○). Normal transmission is indicated by the dashed line.

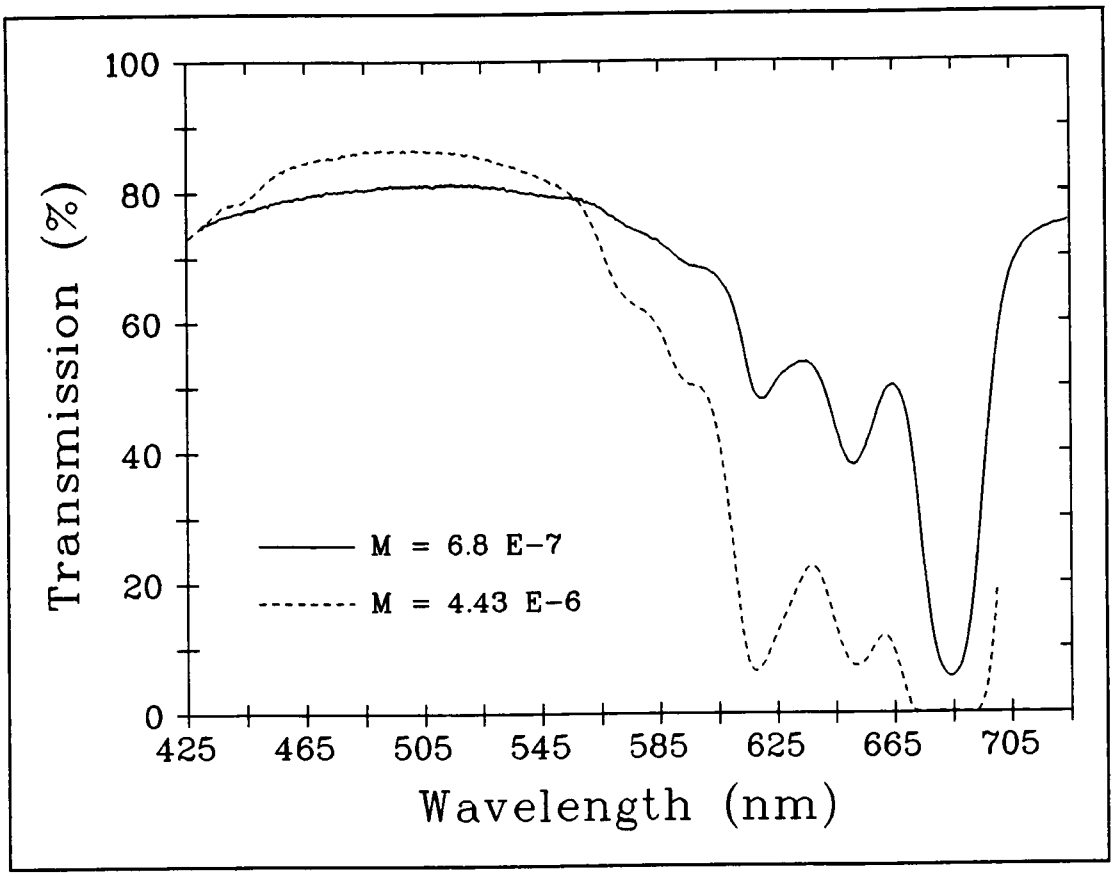

Figure D.1. Transmission of CAP throughout the visible spectrum.

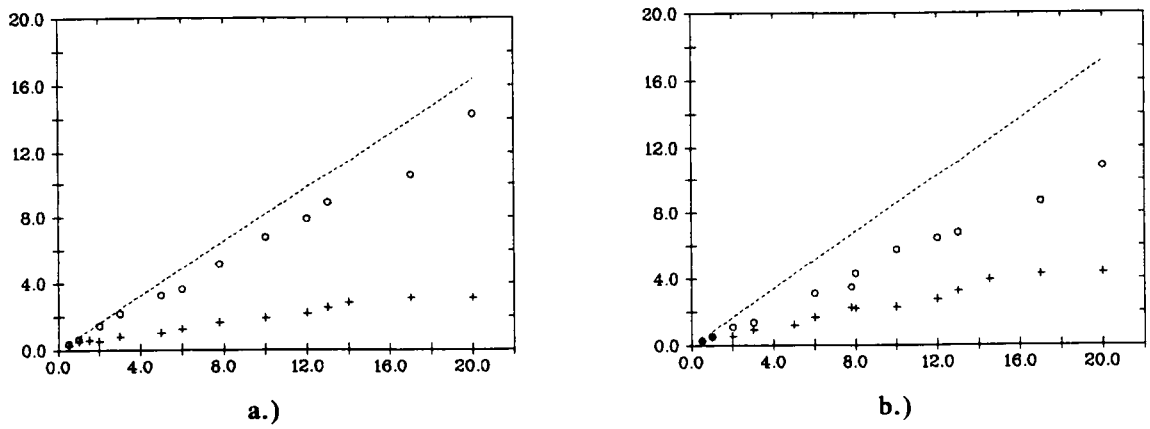

Figure D.2. CAP results for λ = 482 nm. Solution 1 - a, solution 2 - b.

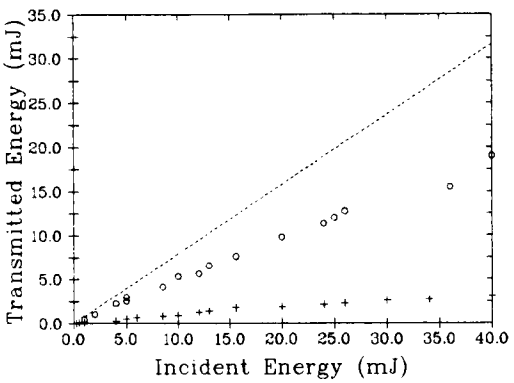

a.)

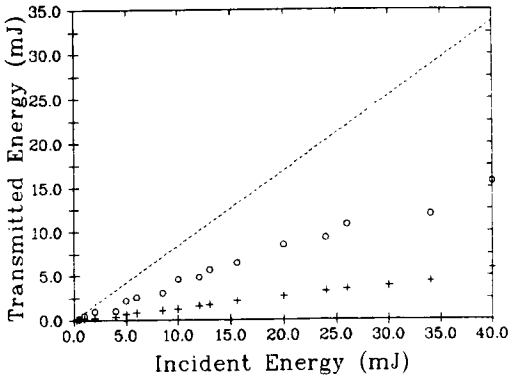

b.)

Figure D.3. CAP results for λ = 532 nm. Solution 1 - a, solution 2 - b.

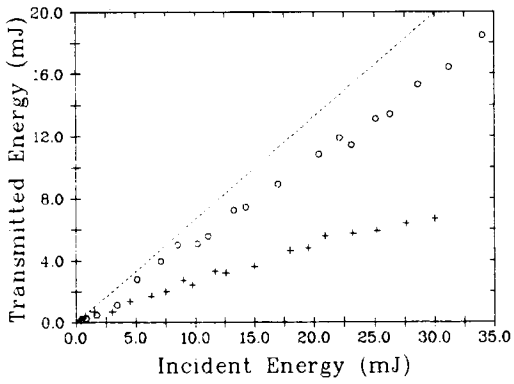

a.)

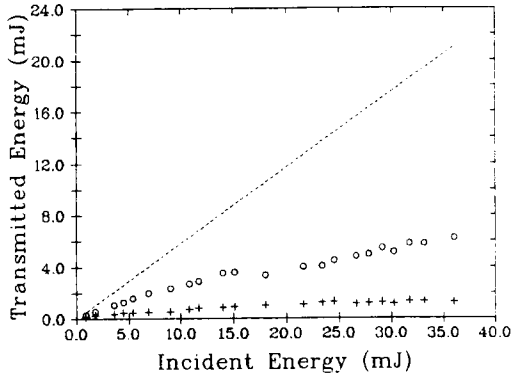

b.)

Figure D.4. CAP results for λ = 585 nm. Solution 1 - a, solution 2 - b.

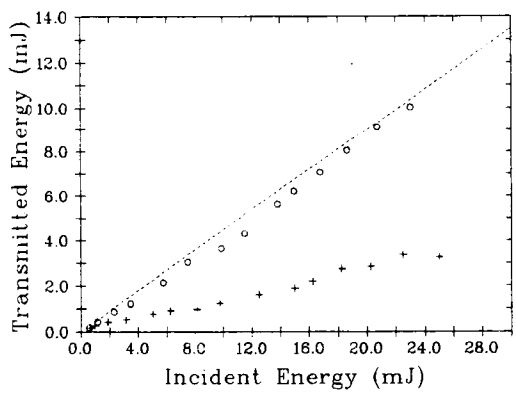

a.)

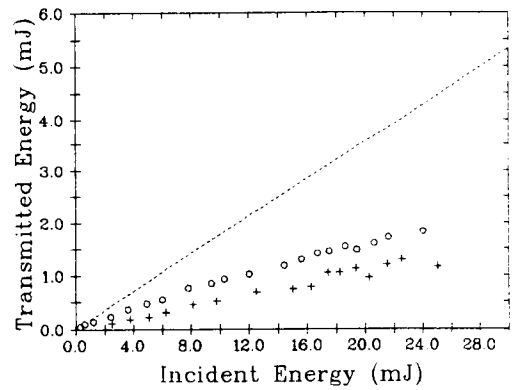

b.)

Figure D.5. CAP results for λ = 630 nm. Solution 1 - a, solution 2 - b.

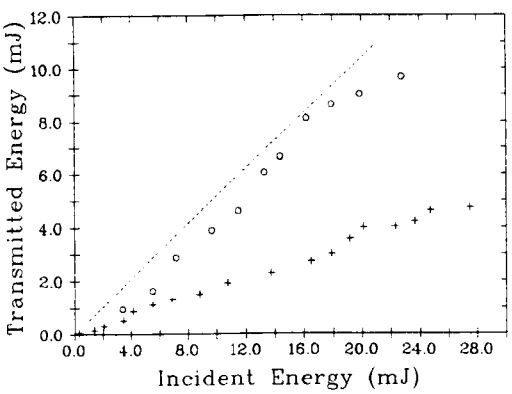

a.)

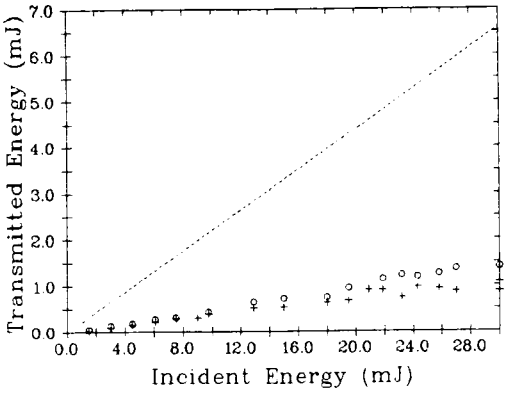

b.)

Figure D.6. CAP results for λ = 640 nm. Solution 1 - a, solution 2 - b.

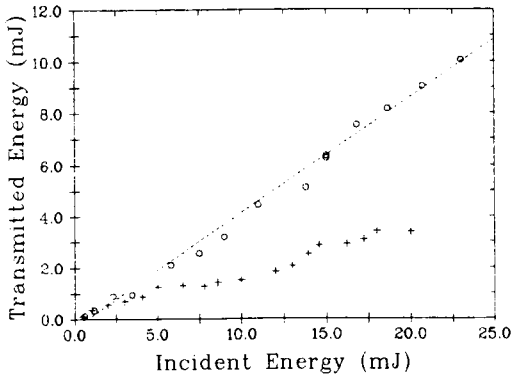

a.)

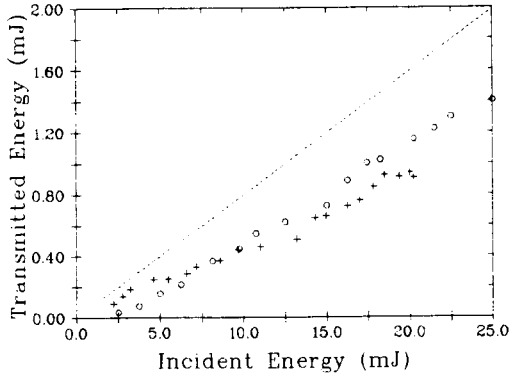

b.)

Figure D.7. CAP results for λ = 660 nm. Solution 1 - a, solution 2 - b.

APPENDIX E

COPPER PHTHALOCYANINE RESULTS

The results for copper pcs show that there is weak absorption of unfocussed light at all wavelengths except for 585 nm. The absorption of focussed light is moderate at all wavelengths. This indicates that copper pcs is not be a good candidate for an attenuator. For all transmission graphs at individual wavelengths, focussed results are symbolized by a (+) and unfocussed by a (○). Normal transmission is indicated by the dashed line.

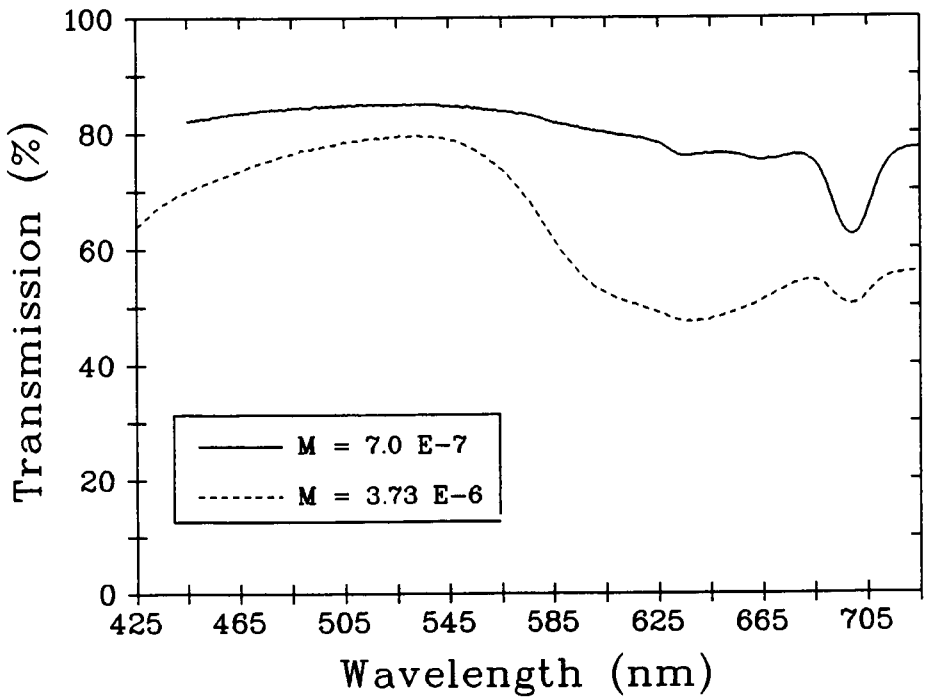

Figure E.1. Transmission of copper pcs.

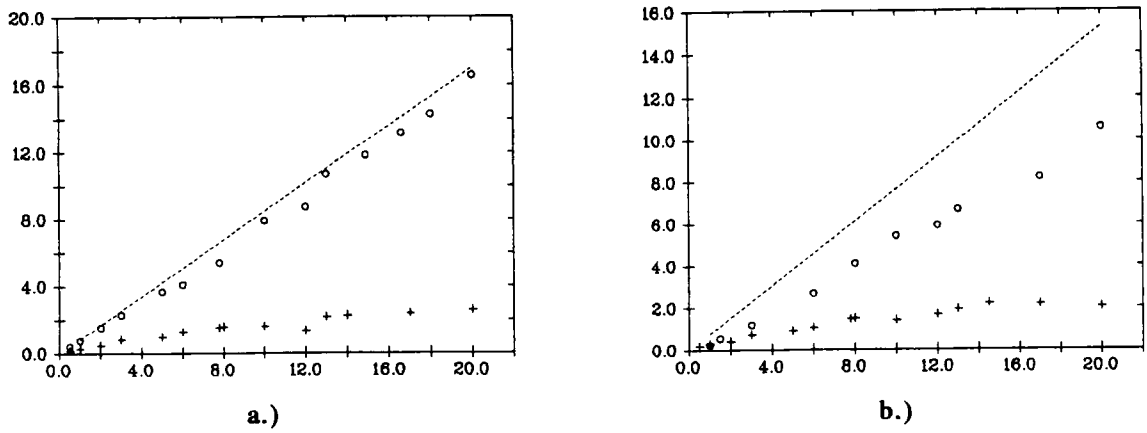

Figure E.2. Transmission of copper pcs at λ = 482 nm. Solution 1 - a, solution 2 - b.

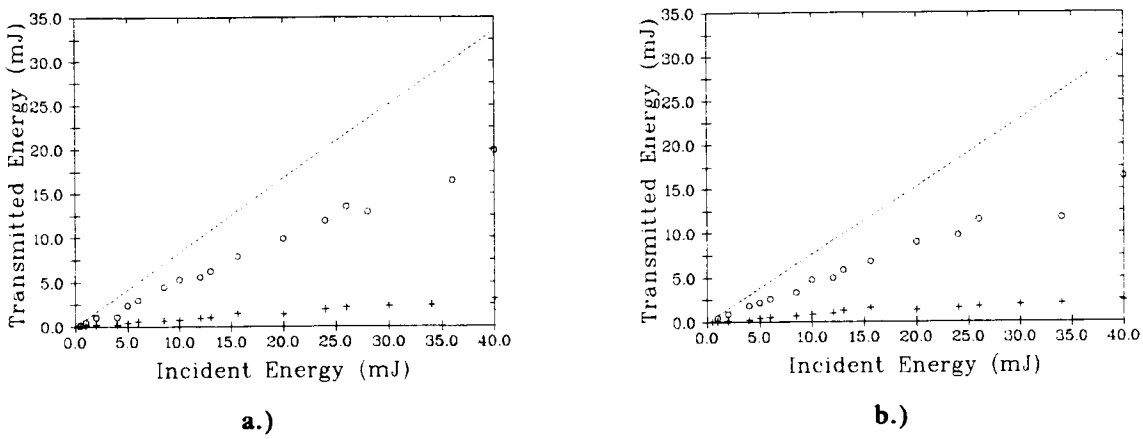

Figure E.3. Transmission of copper pcs at λ = 532 nm. Solution 1 - a, solution 2 - b.

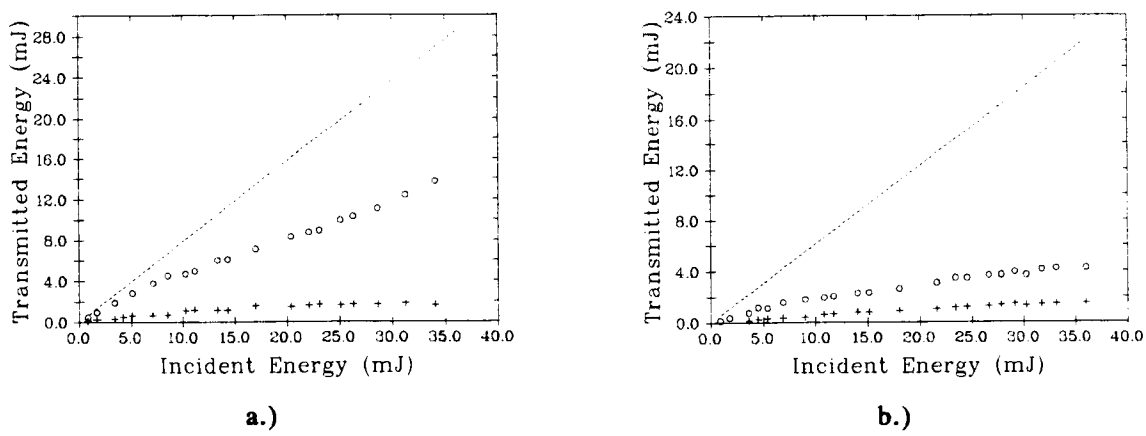

Figure E.4. Transmission of copper pcs at λ = 585 nm. Solution 1 - a, solution 2 - b.

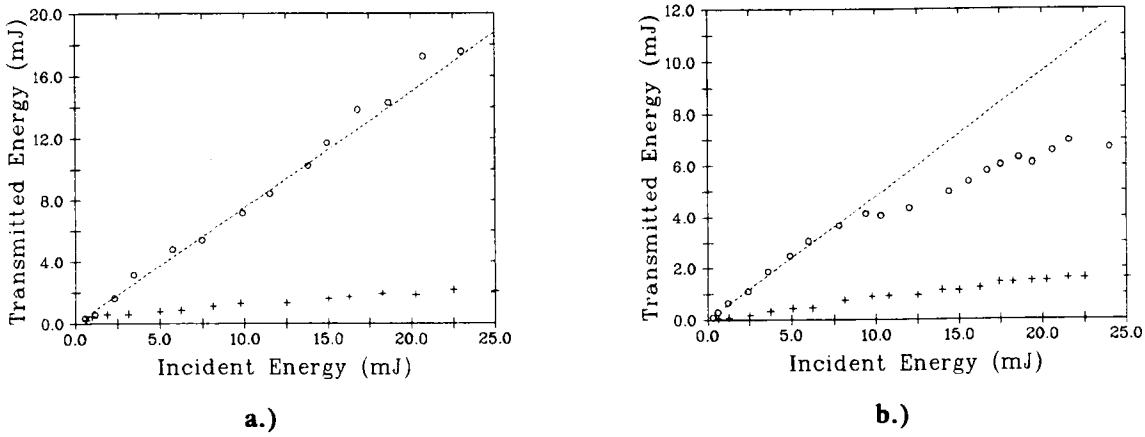

Figure E.5. Transmission of copper pcs at λ= 630 nm. Solution 1 - a, solution 2 - b.

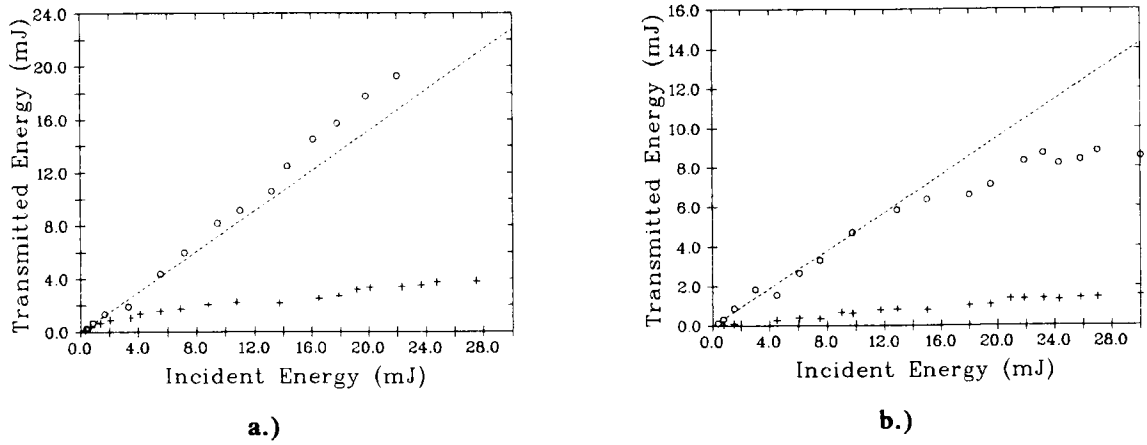

Figure E.6. Transmission of copper pcs at λ = 640 nm. Solution 1 - a, solution 2 - b.

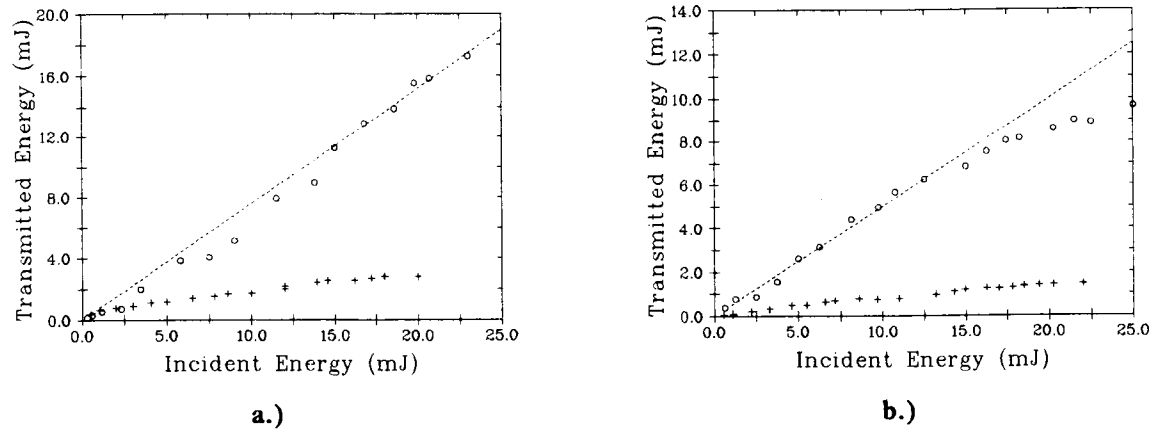

Figure E.7. Transmission of copper pcs at λ = 660 nm. Solution 1 - a, solution 2 - b.

APPENDIX F

PHTHALOCYANINE RESULTS

Normal pcs shows weak absorption of unfocussed light at all wavelengths except for 585 nm and relatively strong absorption of focussed light. Normal pcs is more dependent on the concentration strength than CAP and copper pcs. For all transmission graphs at individual wavelengths, focussed results are symbolized by a (+) and unfocussed by a (o). Normal transmission is indicated by a dashed line.

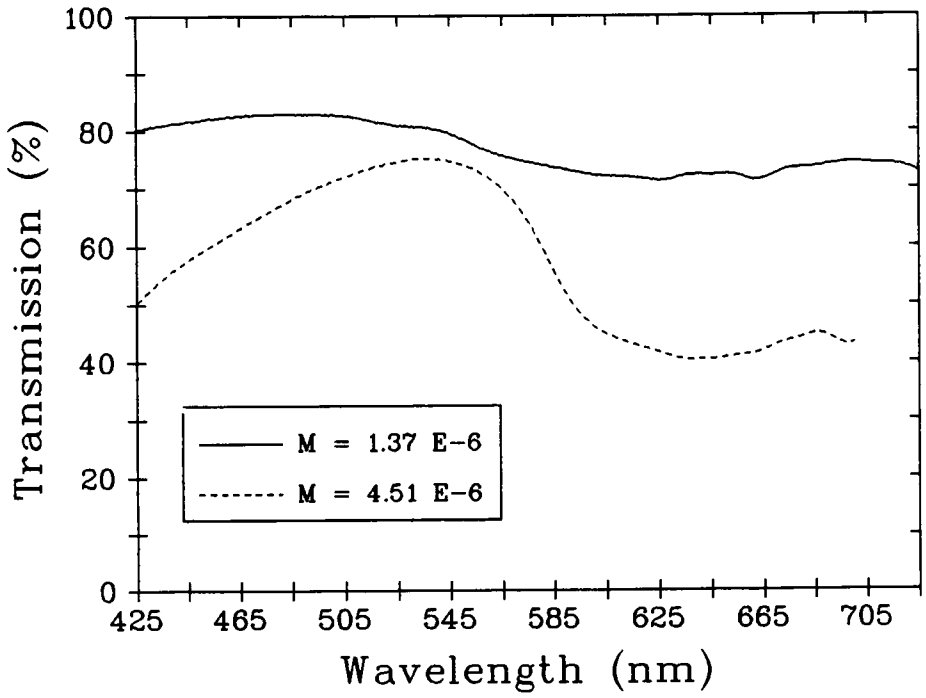

Figure F.1. Transmission of phthalocyanine through visible spectrum.

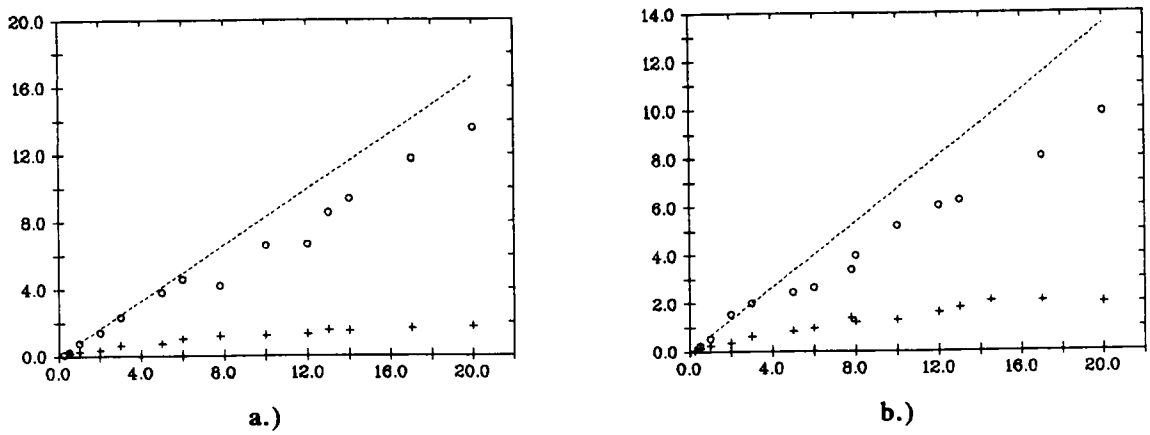

Figure F.2. Transmission of pcs at λ = 482 nm. Solution 1 - a, solution 2 - b.

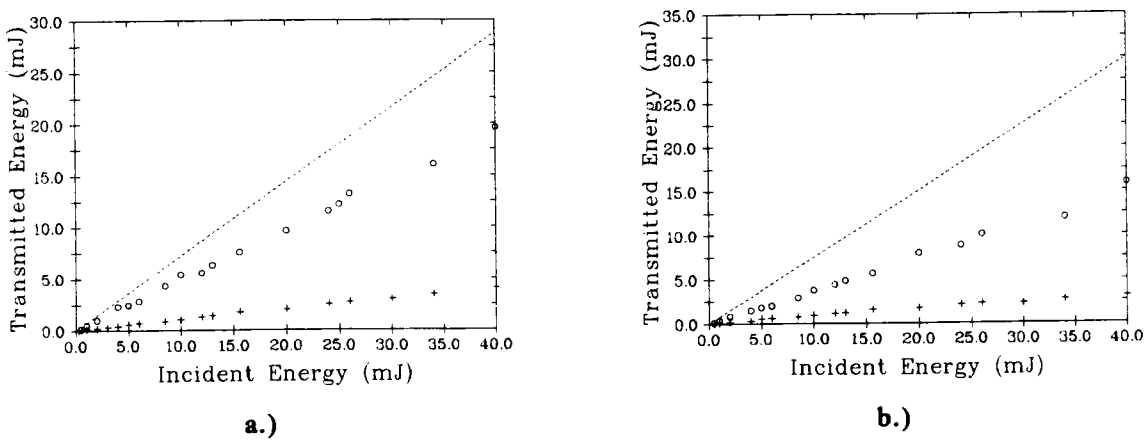

Figure F.3. Transmission of pcs at λ = 532 nm. Solution 1 - a, solution 2 - b.

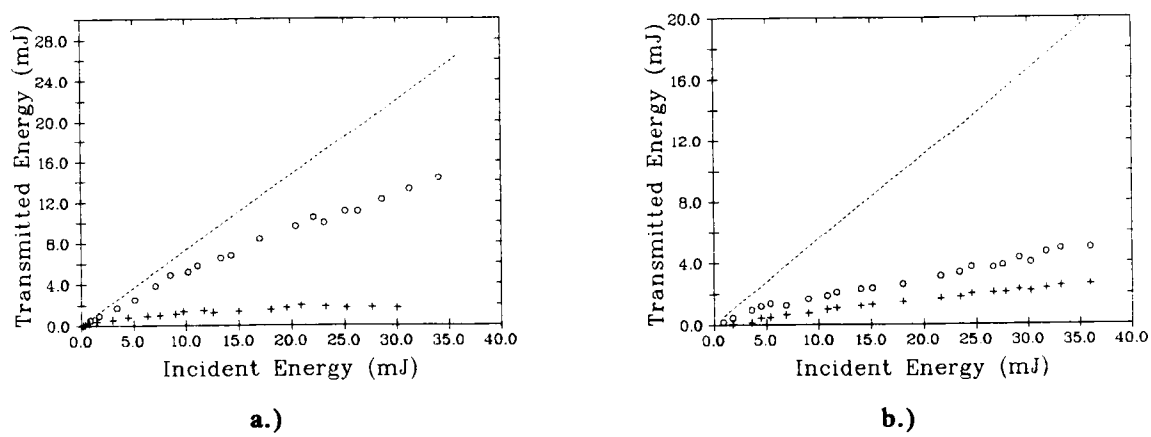

Figure F.4. Transmission of pcs at λ = 585 nm. Solution 1 - a, solution 2 - b.

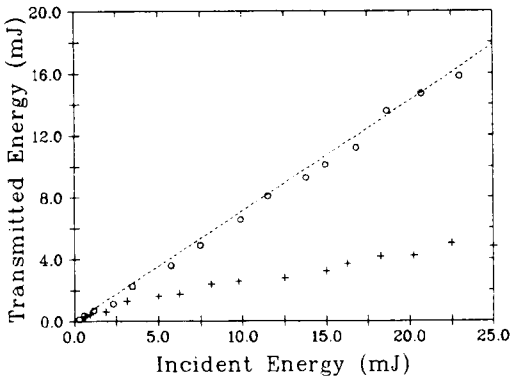

a.)

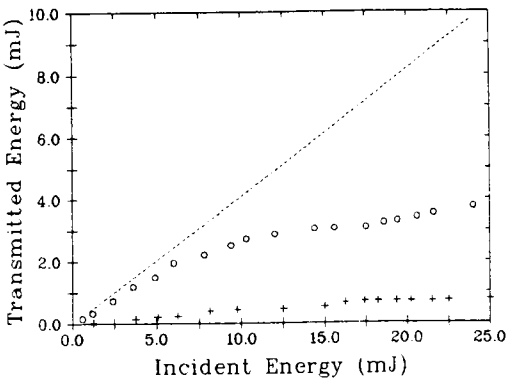

b.)

Figure F.5. Transmission of pcs at λ = 630 nm. Solution 1 - a, solution 2 - b.

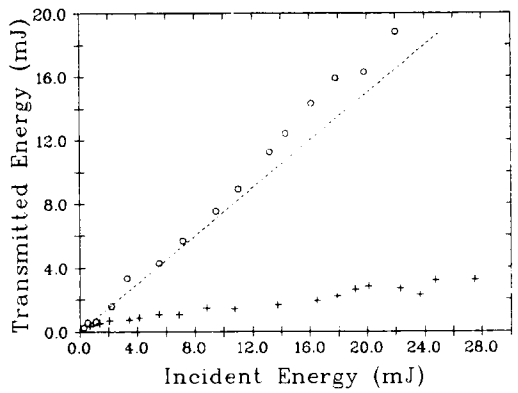

a.)

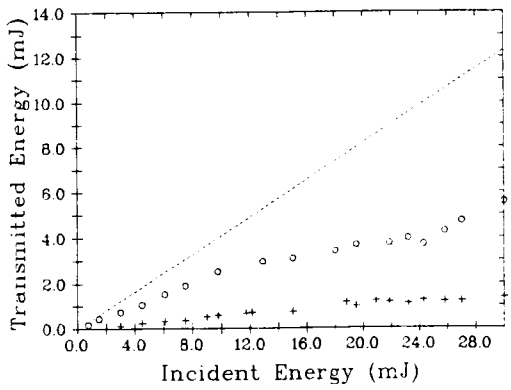

b.)

Figure F.6. Transmission of pcs at λ = 640 nm. Solution 1 - a, solution 2 - b.

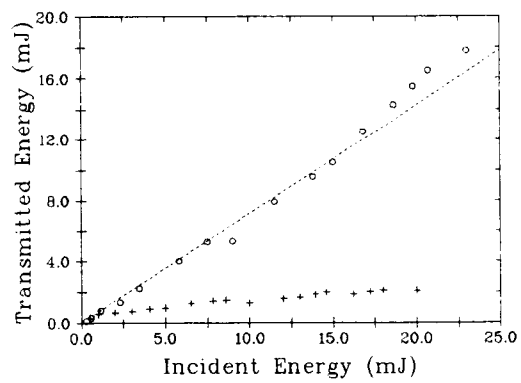

a.)

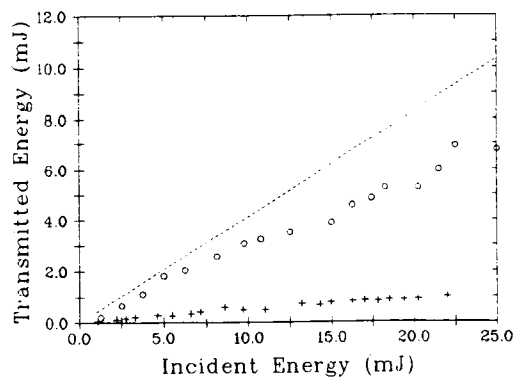

b.)

Figure F.7. Transmission of pcs at λ = 660 nm. Solution 1 - a, solution 2 - b.

APPENDIX G

SODIUM PHTHALOCYANINE RESULTS

Sodium pcs showed the best results overall of all five pcs' tested. Although for some wavelengths, the absorption was weak in the unfocussed state, sodium pcs exhibited the desired optical limiting qualities as outlined in chapter 3. The only linear absorption was revealed at the wavelength of 482 nm using low concentration and unfocussed light. All other tests showed acceptable absorption. For all transmission graphs at individual wavelengths, focussed results are symbolized by a (+) and unfocussed by a (o). Normal transmission is indicated by a dashed line.

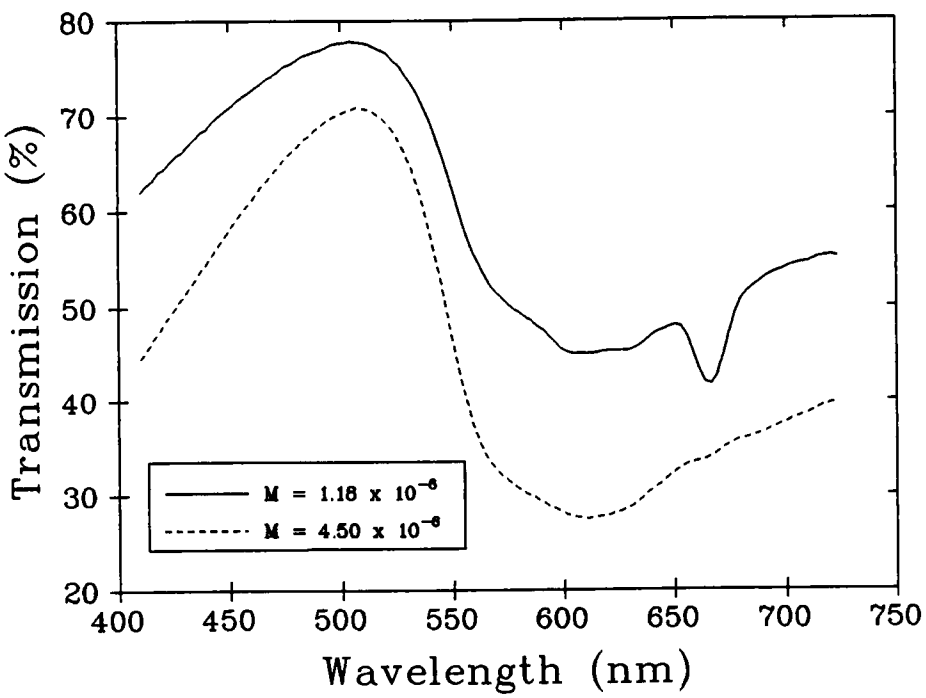

Figure G.1. Transmission of sodium pcs throughout visible spectrum.

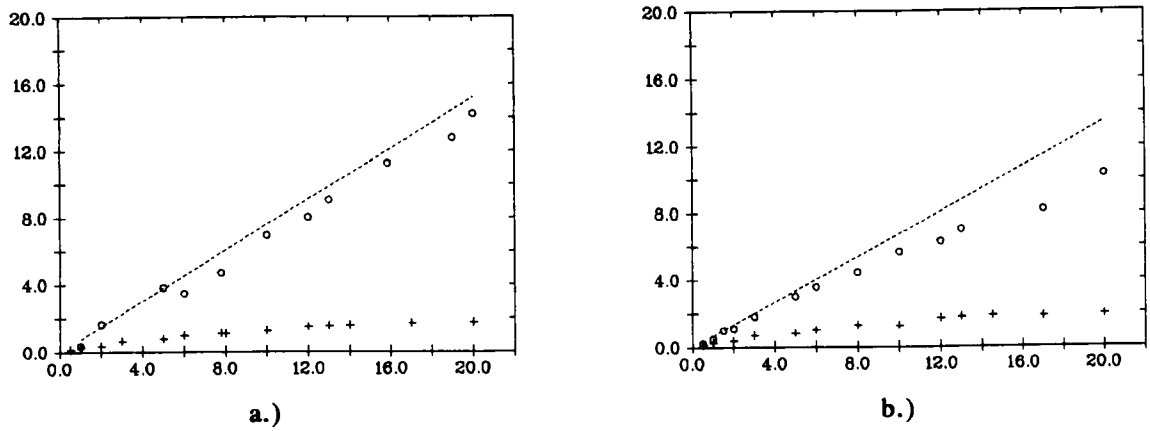

Figure G.2. Transmission of sodium pcs at λ = 482 nm. Solution 1 - a, solution 2 - b.

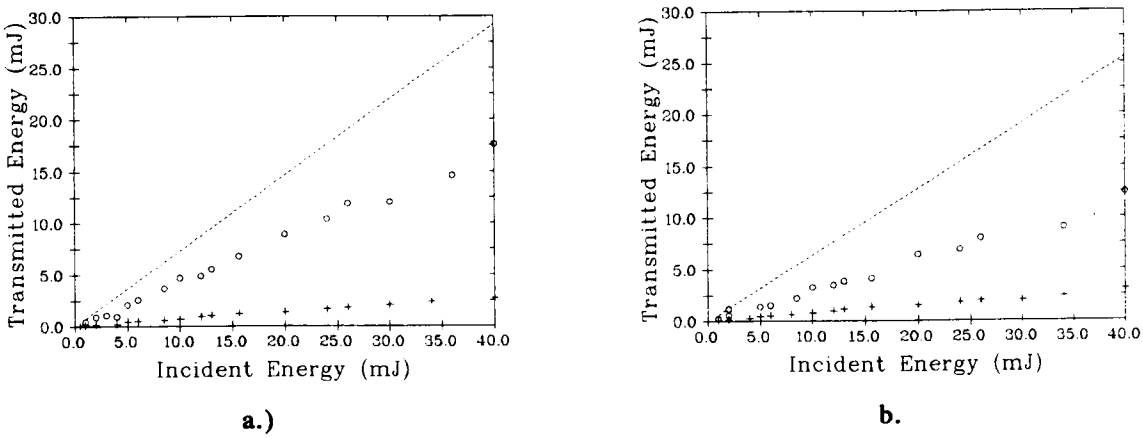

Figure G.3. Transmission of sodium pcs at λ = 532 nm. Solution 1 - a, solution 2 - b.

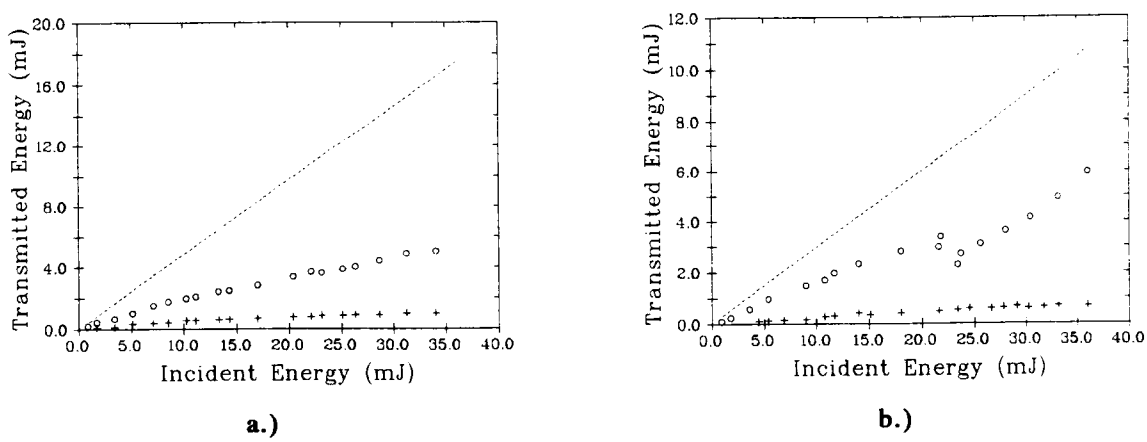

Figure G.4. Transmission of sodium pcs at λ = 585 nm. Solution 1 - a, solution 2 - b.

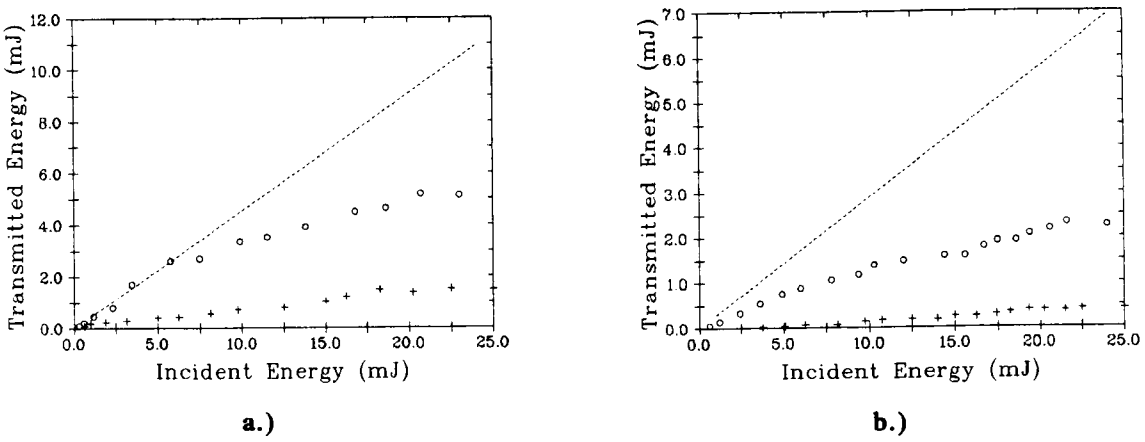

Figure G.5. Transmission of sodium pcs at λ = 630 nm. Solution 1 - a, solution 2 - b.

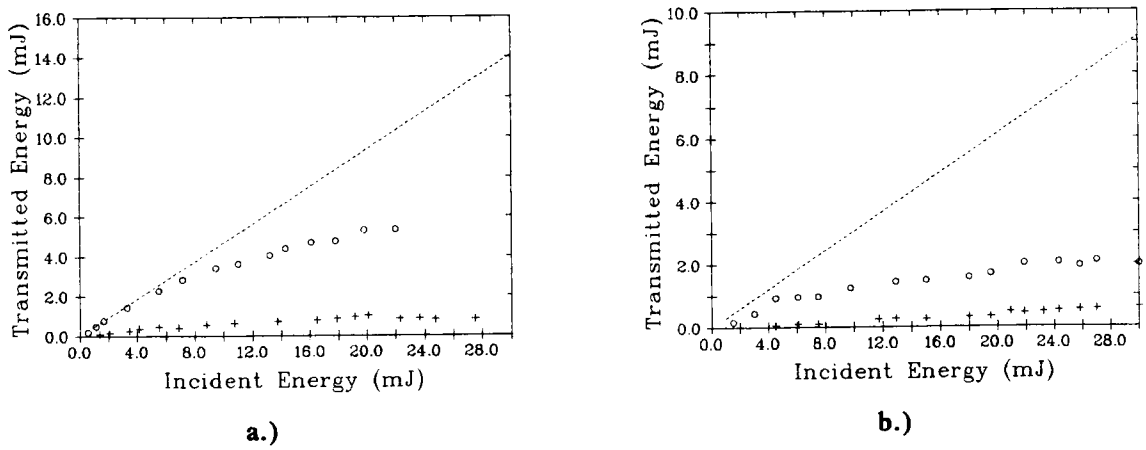

Figure G.6. Transmission of sodium pcs at λ = 640 nm. Solution 1 - a, solution 2 - b.

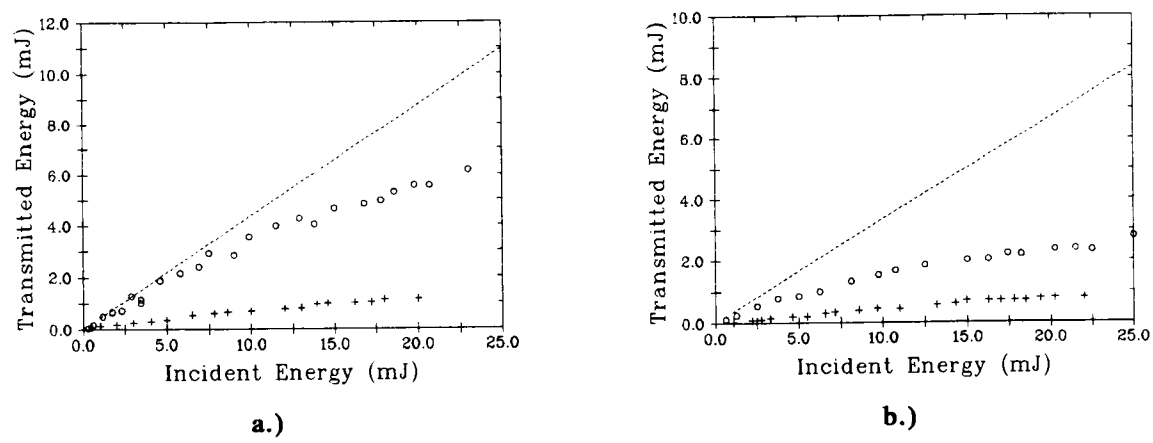

Figure G.7. Transmission of sodium pcs at λ = 660 nm. Solution 1 - a, solution 2 - b.

APPENDIX H.

ZINC PHTHALOCYANINE RESULTS

Zinc pcs, as was the case with sodium pcs, showed acceptable absorption at all wavelengths except 482 nm. The optical limiting mechanism is readily apparent for both the focussed and unfocussed results. For all transmission graphs at individual wavelengths, focussed results are symbolized by a (+) and unfocussed by a (o). Normal transmission is indicated by a dashed line.

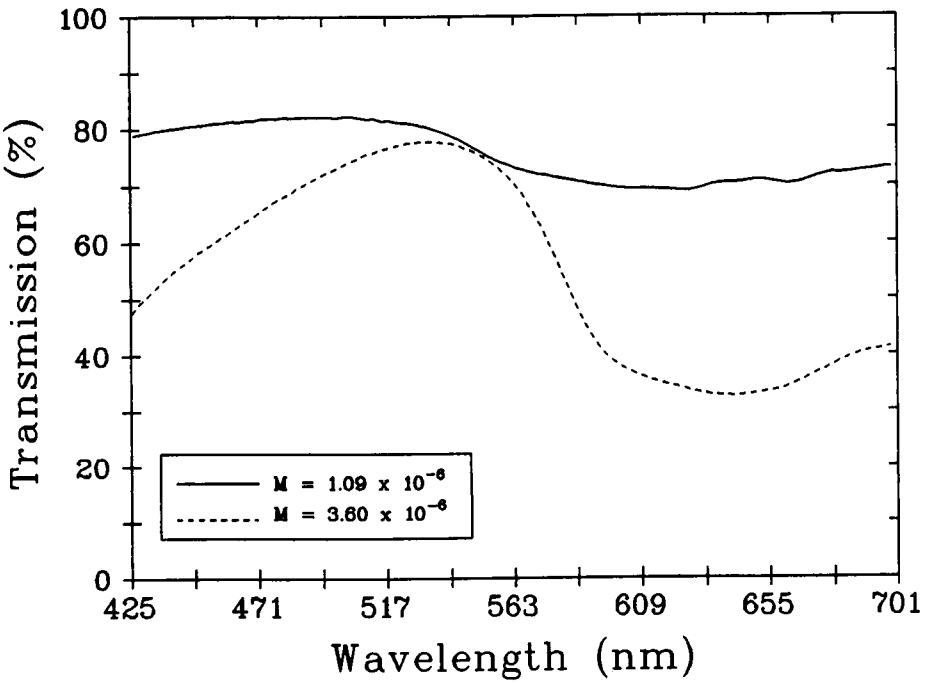

Figure H.1. Transmission of zinc pcs throughout the visible spectrum.

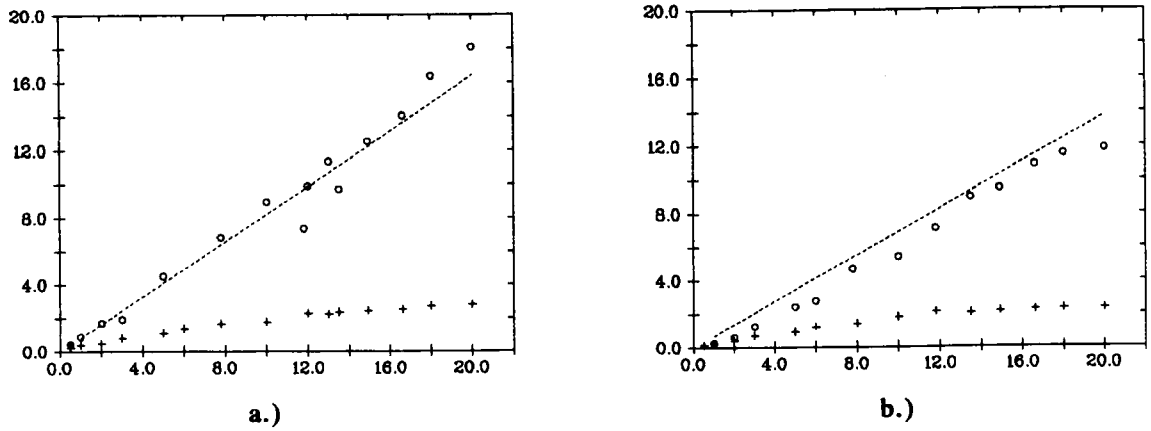

Figure H.2. Transmission of zinc pcs, λ = 482 nm. Solution 1 - a., soln 2 - b.

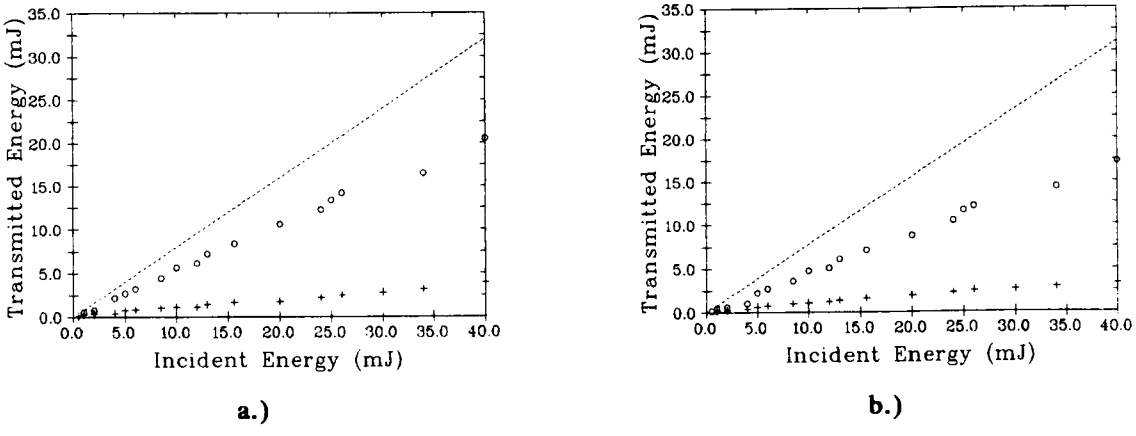

Figure H.3. Transmission of zinc pcs, λ = 532 nm. Solution 1 - a., soln 2 - b.

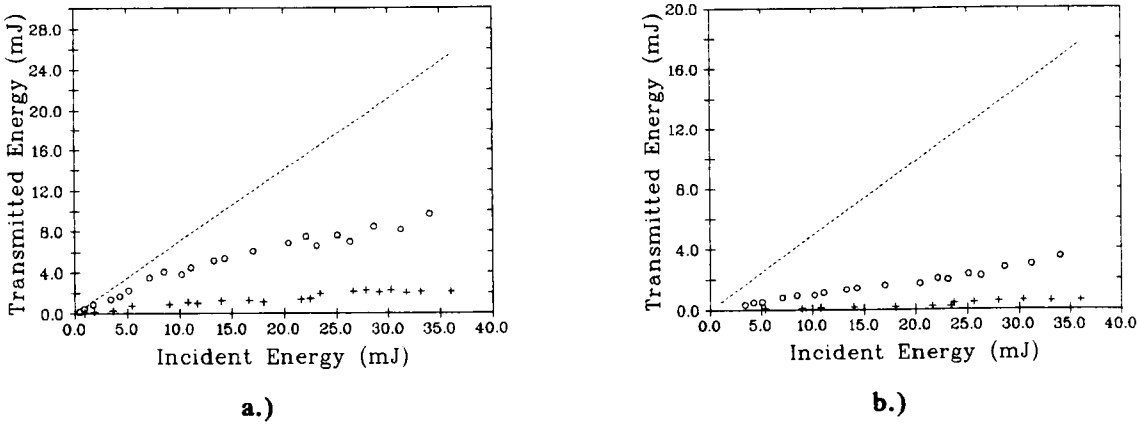

Figure H.4. Transmission of zinc pcs at λ = 585 nm. Solution 1 - a., soln 2 - b.

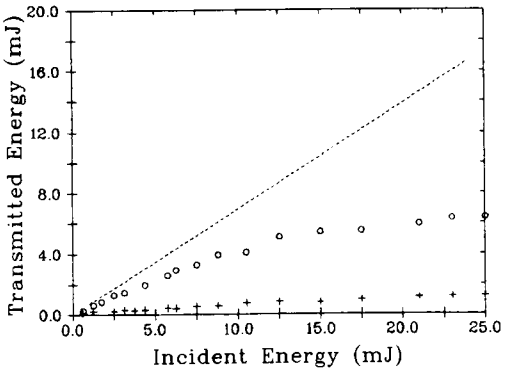

a.)

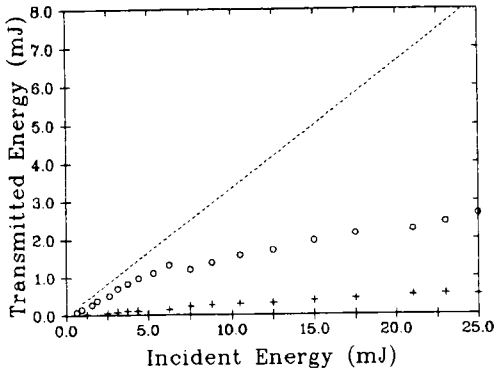

b.)

Figure H.5. Transmission of zinc pcs at λ = 630 nm. Solution 1 - a., soln 2 - b.

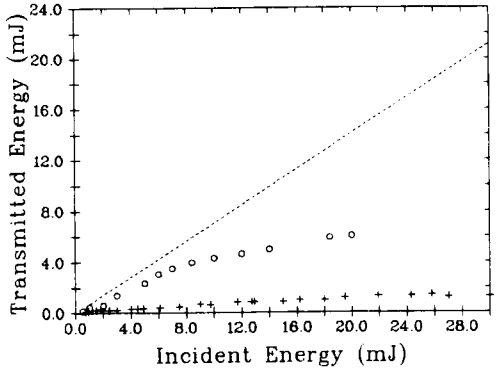

a.)

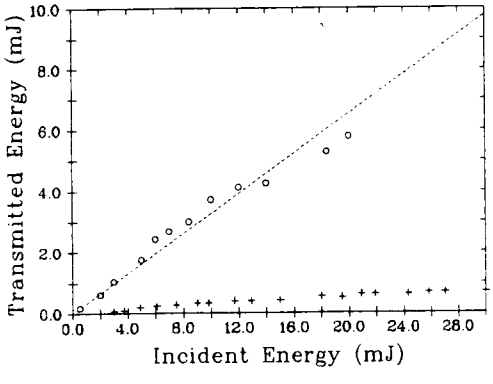

b.)

Figure H.6. Transmission of zinc pcs at λ= 640 nm. Solution 1 - a., soln 2 - b.

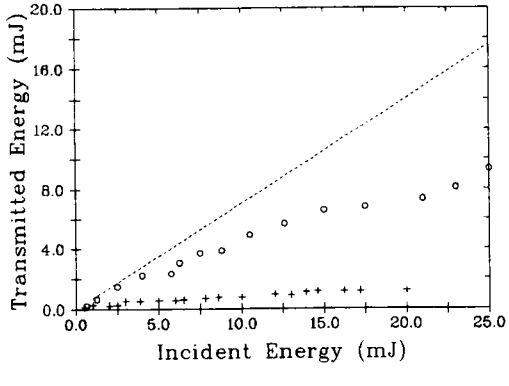

a.)

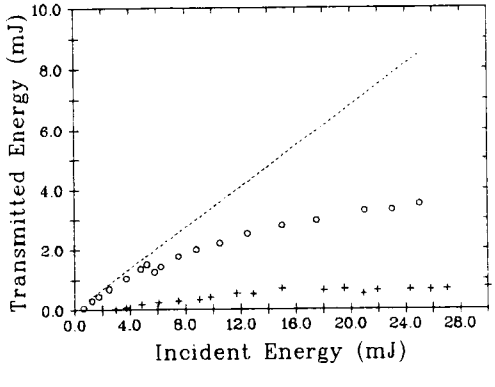

b.)

Figure H.7. Transmission of zinc pcs at λ = 660 nm. Solution 1 - a., soln 2 - b.

VITA

James Jack DiCillo was born in Cleveland, Ohio on July 5, 1960. After graduating from high school, he attended John Carroll University for three years, majoring in Economics. He then spent four years in the United States Army working with nuclear weapons. Upon his discharge in 1985, he returned to school and graduated from Cleveland State University in 1989 with a Bachelor of Science in Physics. The following autumn, he started graduate school at the University of Tennessee. His research was conducted at Oak Ridge National Laboratory from January 1991 until his graduation in August, 1992. He graduated with a Master of Science degree in Physics.